ACCEPTED VERSION

"This is the peer reviewed version of the following article:

John W. Counts and Kathryn J. Amos

Sedimentology, depositional environments and significance of an Ediacaran salt-withdrawal minibasin, Billy Springs Formation, Flinders Ranges, South Australia

Sedimentology, 2016; 63(5):1084-1123

© 2015 The Authors. Sedimentology © 2015 International Association of Sedimentologists

which has been published in final form at http://dx.doi.org/10.1111/sed.12250

This article may be used for non-commercial purposes in accordance with Wiley Terms and Conditions for Self-Archiving."

PERMISSIONS

http://olabout.wiley.com/WileyCDA/Section/id-828039.html

Publishing in a subscription based journal

Accepted (peer-reviewed) Version

The accepted version of an article is the version that incorporates all amendments made during the peer review process, but prior to the final published version (the Version of Record, which includes; copy and stylistic edits, online and print formatting, citation and other linking, deposit in abstracting and indexing services, and the addition of bibliographic and other material.

Self-archiving of the accepted version is subject to an embargo period of 12-24 months. The embargo period is 12 months for scientific, technical, and medical (STM) journals and 24 months for social science and humanities (SSH) journals following publication of the final article.
- the author's personal website
- the author's company/institutional repository or archive
- not for profit subject-based repositories such as PubMed Central

Articles may be deposited into repositories on acceptance, but access to the article is subject to the embargo period.

The version posted must include the following notice on the first page:

"This is the peer reviewed version of the following article: [FULL CITE], which has been published in final form at [Link to final article using the DOI]. This article may be used for non-commercial purposes in accordance with Wiley Terms and Conditions for Self-Archiving."

The version posted may not be updated or replaced with the final published version (the Version of Record). Authors may transmit, print and share copies of the accepted version with colleagues, provided that there is no systematic distribution, e.g. a posting on a listserve, network or automated delivery.

There is no obligation upon authors to remove preprints posted to not for profit preprint servers prior to submission.

28 June 2017

http://hdl.handle.net/2440/97759

Received Date : 27-Mar-2015

Revised Date : 08-Oct-2015

Accepted Date : 27-Oct-2015

Article type : Original Manuscript

SEDIMENTOLOGY, DEPOSITIONAL ENVIRONMENTS AND SIGNIFICANCE OF AN EDIACARAN SALT-WITHDRAWAL MINIBASIN, BILLY SPRINGS FORMATION, FLINDERS RANGES, SOUTH AUSTRALIA

JOHN W. COUNTS* and KATHRYN J. AMOS

(1) Australian School of Petroleum, University of Adelaide, Adelaide, SA, 5005, Australia;

john.counts@adelaide.edu.au; kathryn.amos@adelaide.edu.au

*Corresponding author.

Running Title: EDIACARAN MINIBASIN SEDIMENTOLOGY

Running Authors: COUNTS AND AMOS

Keywords: Ediacaran, glacial, mass flow, Neoproterozoic, salt withdrawal

ABSTRACT (A)

The late Ediacaran Billy Springs Formation is a little-studied, mudstone-dominated unit deposited in the Adelaide Rift Complex of South Australia. Sediments are exposed in an approximately 11 km x 15 km wide synclinal structure interpreted as a salt-withdrawal minibasin. The stratigraphic succession is characterized by convolute-laminated slump

This is an Accepted Article that has been peer-reviewed and approved for publication in the *Sedimentology*, but has yet to undergo copy-editing and proof correction. Please cite this article as an “Accepted Article”; doi: 10.1111/sed.12250

deposits, rhythmically-laminated silty mudstones, rare diamictites and fining-upward turbidite lithofacies. Lithofacies are the product of deposition in a deepwater slope or shelf setting, representing one of the few such examples preserved within the larger basin. Although exact correlations with other formations are unclear, the Billy Springs Formation probably represents the distal portion of a highstand systems tract, and is overlain by coarser sediments of the upper Pound Subgroup. Diamictite intervals are interpreted to be the product of mass flow processes originating from nearby emergent diapirs, in contrast to previous studies that suggest a glacial origin for extrabasinal clasts. Within the spectrum of outcropping minibasins around the world, the sediments described here are unique in their dominantly fine-grained nature and overall lithological homogeneity. Exposures such as these provide an opportunity to better understand the sedimentological processes that operate in these environments, and provide an analogue for similar settings in the subsurface that act as hydrocarbon reservoir-trap systems.

INTRODUCTION (A)

Although salt-withdrawal minibasins form a significant portion of the world's hydrocarbon-bearing strata, outcrop exposures of these types of environments are relatively limited in number (Table 1); hence, they are understudied with regard to detailed mesoscale sedimentation processes and products that make up minibasin fill. The purpose of this paper is to describe and interpret the Billy Springs Formation, a succession of predominantly clastic sediments deposited in a depocentre interpreted as a salt-withdrawal minibasin on the late Ediacaran (Neoproterozoic) passive margin of southern Australia. These sediments are well-exposed in the northern Flinders Ranges, allowing detailed outcrop observations that can be used to better understand similar deposits in the subsurface around the world.

Salt-withdrawal minibasins are found throughout the world in a wide range of depositional settings. In the marine realm, they often create circular or elliptical topographic lows on the seafloor (Bouma & Bryant, 1995; Brown et al., 2004; Mallarino et al., 2006), and many contribute to petroleum trapping mechanisms at depth (Pilcher et al., 2011). Intraslope minibasin deposits are often dominated by gravity-driven flow (especially turbidites; e.g. Lamb et al., 2006) and can trap coarser-grained sediments originating from slope canyons and delta fans (Winker, 1996; Prather, 2000). Previous detailed studies of minibasin sedimentation in ancient deposits come primarily from core data (e.g. Mannie et al., 2014) as well as limited outcrops around the world, including elsewhere in the Flinders Ranges of Australia (see Table 1 and references therein). Table 1 presents a summary of published outcrop studies of salt-withdrawal minibasins that include at least some description of the sedimentology of the basin fill deposits. The formation, infilling history and stratigraphic architecture of these types of basins have also been studied in detail in the Gulf of Mexico and other offshore settings in recent years through subsurface data (e.g. Prather, 2000; Madof et al., 2009; Pilcher et al., 2011; and many others). The present study seeks to examine the type of sedimentary fill and history of sedimentation of a Neoproterozoic minibasin from a process and lithofacies perspective, on a different scale than typically seen in either seismic, core or wireline data.

In the Flinders Ranges, numerous individual salt diapirs (preserved as dolomitic breccias) and several kilometres of basin fill are well-exposed at the surface (Preiss, 1987; Dyson, 1996). Folding and uplift in the Late Cambrian allows for both cross-sectional and plan view examination of diapirs and adjacent strata. The Umberatana Syncline, previously interpreted as a salt-withdrawal minibasin (Dyson, 2005; Rowan & Vendeville, 2006), exposes sediments of the Billy Springs Formation, a mudstone-dominated lithostratigraphic unit that has been hypothesized to represent the deepwater or downslope equivalent of shallow marine coarser sediments to the south (Von der Borch & Grady, 1982). Previous studies of this unit have been limited in scope; this article presents the first detailed description and interpretation of the sedimentary lithofacies, depositional environments and significance of the Billy Springs Formation. The primary aim of this paper is to provide a case study in minibasin sedimentation, thereby demonstrating an unambiguous record of the depositional processes and products involved in the infilling of a Precambrian minibasin. Specific research goals of this study are as follows:

- Documentation of the succession of sediments in the minibasin, and determination of the processes responsible for their emplacement and whether depositional characteristics are a result of minibasin formation itself, or of external forces. This is accomplished through field classification of sediments into lithofacies, laboratory analysis to better understand lithological properties, interpretation of lithofacies based on established sedimentological principles and the recognition of the larger geological context in which the minibasin lies.
- Incorporation of the Billy Springs Formation into a larger palaeogeographic and sequence stratigraphic context, which can be used to better understand the history of the region and of Precambrian Australia as a whole. Outlining the evidence for the Umberatana Syncline as a salt-withdrawal minibasin.
- Using both the observations herein and existing research, to determine how this minibasin compares to others described in the geological record, and to those that are parts of productive hydrocarbon systems. What are the features seen here that are also frequently noted in minibasins elsewhere? Can this

minibasin be accurately used as an analogue to predict the properties of some subsurface deposits?

Answers to these questions require a basic understanding of the Billy Springs Formation, which is necessary for any further insight into its larger significance.

Although salt-withdrawal minibasins have been well-studied in the subsurface, they have generally not been regarded as unique depositional environments in a sedimentological sense, with a few recent exceptions (e.g. Banham & Mountney, 2013a, 2013b, 2014; Ribes et al., 2015; Venus et al. 2015). Although much is dependent on surroundings, detailed studies of minibasins in a diverse array of settings can be collated to reveal common depositional processes and stratigraphic trends, allowing generalizations to be made that can ultimately result in predictive models for minibasin sedimentology. In combination with geophysical and core data, outcrops are key to a full understanding of the overall stratigraphic architecture of these deposits. All new outcrop studies, therefore, provide new information on the distribution and lateral variability of lithofacies in these deposits.

GEOLOGICAL SETTING (A)

During much of the Neoproterozoic, the Adelaide Rift Complex was a rift basin occupying part of Rodinia, a large supercontinent that existed until approximately 750 Ma (Li et al., 2008; Bogdanova et al. 2009). Most reconstructions based on palaeomagnetic data place Australia in low latitudes, between the palaeoequator and 30 degrees north (Li et al., 2008). By the late Ediacaran, Rodinia had already broken apart, and Australia was part of a smaller subcontinent (Johnson, 2013).

Throughout basin history, the Adelaide Rift Complex was adjacent to the Gawler Craton to the west and the smaller Curnamona Craton to the east (present-day orientation; Fig 2). Both of these provinces are composed primarily of pre-rift Proterozoic igneous rocks, which were relatively stable during basin formation and fill and were periodically subaerially exposed (Drexel, 1993). To the south and east, the margin was probably connected to the larger ocean, although the degree of restriction and connectivity varied with sea-level and local tectonics over time (Preiss, 1987). Basal units in the basin fill are characterized by volcanics and evaporites, and were probably deposited in an incipient rift system. By the Ediacaran, it is generally accepted that the rift had evolved into a passive continental margin (eastward-facing in the present day), with the large Curnamona Craton possibly forming a large island offshore (Preiss 1990), as Australia east of the Tasman Line had not yet amalgamated onto the older western portion of the subcontinent (Johnson, 2013). The northern extent of the rift complex may have been limited by the Muloorina Ridge, a basement gravity high that may have been exposed prior to the latest Ediacaran, although this remains speculative (Preiss, 1990). During the later Ediacaran, sediments thicken dramatically to the north, with the Pound Subgroup reaching 2500 m in the Gammon Ranges area (Gehling, 1982), compared to 813 m thick in the type section in Bunyeroo Gorge (Forbes, 1971).

The basin fill is complex, with numerous (>100) formal lithostratigraphic units deposited roughly from the early Cryogenian (*ca* 830 Ma; Preiss, 2000) to the Middle Cambrian (Drexel, 1993; Fig. 3). Infilling took place in multiple phases, beginning with the early rift sediments of the Callanna Group and culminating with the uplift and folding of the basin fill during the Cambrian–Ordovician Delamerian Orogeny (Preiss, 1987). In addition to larger-scale rifting episodes, syndepositional extensional faulting is recognized throughout the basin. Salt diapirs originating from Callanna Group evaporites were also active during deposition of later basin fill, with indications of synsedimentary diapir activity as early as the Sturtian glacial episode (represented by the Burra Group; see Fig. 3) and continuing through to the cessation of deposition in the Early Cambrian (Dalgarno & Johnson, 1968). Diapir mobilization was probably caused by loading of the thick accumulation of sediments in the narrow, rapidly subsiding rift-sag basin, although Davison et al. (1996) note that little or no overburden is required to initiate salt movement; however, this depends on the nature of the evaporite matrix and whether it is mixed with carbonate or clastic lithologies. Exposures of the Callanna Group *in situ* are found only in the distant outliers and margins of the basin; the unit is known primarily from allochthonous blocks, sometimes hundreds of metres in diameter, found within diapiric breccia (Preiss, 1987). No salt remains at the surface, with diapir matrix having been replaced by a fine-grained dolomite, although pseudomorphs of halite crystals are common and the evaporite origin of these bodies is well-established (Dalgarno & Johnson, 1968). The Billy Springs Formation forms the one of the latest Precambrian (Ediacaran) units in the Adelaide Rift Complex, and like many of the sediments in the basin, its distribution and internal character are likely to be influenced by the continued mobilization of underlying salt.

BACKGROUND (A)

The Billy Springs Formation is exposed only in two areas in the northern Flinders Ranges, the Umberatana and Mount Freeling Synclines, which lie north and west of Arkaroola Village (Fig. 4). Few in-depth geological studies have previously been conducted on these exposures. Previous sedimentological interpretations of this interval generally favour a marine lower shelf or slope depositional environment for the Billy Springs deposits (e.g. Von der Borch & Grady, 1982; Jenkins, 2011). Dibona et al. (1990) note that the shelf-slope transition in the underlying Wonoka Formation lies only *ca* 15 km south of the Umberatana Syncline, which also contains kilometre-scale incised canyons near the study area. Exact stratigraphic correlations with other units in the basin have varied with different authors, although it is generally agreed upon that Billy Springs Formation sediments tie to either the upper Wonoka Formation, the lower Bonney Sandstone, or both (Coats & Blissett, 1971; Reid, 1992; Pell et al., 1993; Von der Borch & Grady, 1982; Table 2). In addition, various authors have differently interpreted the presence of large clasts within mudstones and siltstones of the Billy Springs Formation as the product of either glacial processes (Jenkins, 2011) or mass flow deposits (Von der Borch et al., 1982). Previous investigations have recognized the basic depositional framework of the Billy Springs Formation, but have mostly been brief or reconnaissance studies in specialty journals, have focused on exposures elsewhere or have not been published in peer-reviewed literature. Detailed sedimentology, petrography and provenance, as well as the larger significance of the formation, remain poorly understood. The present study seeks to incorporate observations from these previous studies with this work in order to create a more comprehensive model for the evolution of minibasin fill over time.

FIELD AND LABORATORY METHODOLOGY (A)

This study focuses on the lower unit of the Billy Springs Formation exposed in the Umberatana Syncline, on the Umberatana Station property in the northern Flinders Ranges. Two relatively continuous sections were measured for this study, named Old Station Creek North (OSCN) and Old Station Creek South (OSCS; locations shown in Fig. 4). These sections comprise over 1370 m and 316 m of vertical thickness, respectively. Both sections were measured from the base of the Billy Springs Formation, as determined from field observations and the 1 : 63360 Umberatana geological map sheet (Campana et al., 1961).

Exposures were relatively continuous, with beds dipping approximately 10 to 25 degrees (magnitude) to the east in the section OSCN, and 50 to 65 degrees to the north-west at the base of section OSCS, becoming shallower up section to 10 to 20 degrees dip magnitude. In each section, lithologies were closely examined with regard to bed thickness, bed continuity, grain size and sedimentary structures, and samples were taken at selected representative intervals for further analysis.

Polished thin sections of selected samples were analysed for mineralogy using both traditional petrography and QEMSCAN (Quantitative Evaluation of Minerals by Scanning Electron Microscopy) methodology, performed by staff at the University of South Australia. The QEMSCAN method uses both backscattered electron (BSE) intensity and low-count energy dispersive X-ray spectra (EDX) to automatically identify the composition of a selected point against an internal mineral database.

OBSERVED LITHOFACIES: DESCRIPTION, DISTRIBUTION AND INTERPRETATION (A)

Stratigraphic sections are presented in Fig. 5, and brief descriptions of stratigraphic units are presented in Table 3 (OSCS) and Table 4 (OSCN). The Billy Springs Formation contains four distinct lithofacies that occur throughout the succession, in varying degrees of abundance: (i) planar-laminated silty mudstone; (ii) convolute-laminated silty mudstone;(iii) matrix-supported diamictite; and (iv) tabular-bedded sandstone. Two facies associations are described. Individual lithofacies are often contained in discrete units, separated by sharp contacts, but more gradational transitions also exist. The formation is dominated by silty mudstones, often containing millimetre-scale planar interlaminae of very fine sands and silts ('laminated' defined here as being stratification <1 cm in thickness). In both sections, sand-dominated beds are more abundant in stratigraphically higher intervals, with decimetre-scale, fine-grained sandstones interbedded with planar mudstones similar to those seen below (Fig. 5). Although measured sections are partially correlative, significant differences in lithofacies distribution exist between the two (Fig. 5). These are described in more detail below.

Planar-laminated silty mudstone (Lithofacies *Mpl*) (B)

Description (C)

This lithofacies is dominated by silt-sized and clay-sized particles. Individual laminae are a product of textural and compositional differences (Figs 6A and 7A), although millimetre-scale laminae are not always present and are commonly not visible in thin section (Fig. 6B). Based on thin section observations, overall silt content varies considerably. The QEMSCAN mineralogical analysis of a single finely laminated interval (Fig. 7) reveals that these sediments are composed primarily of quartz, clay minerals and micas. Layers that are lighter coloured in hand sample have a higher percentage of coarse silt-sized, quartz grains, while finer-grained, darker laminae are dominated by clays and micas. Neither type of laminae is consistently thinner or thicker than the other. Detrital carbonate and feldspar grains are interspersed throughout the sample, and are slightly more common in coarser laminae, because most of them are closer in size to the silt-sized grains that make up coarser intervals. Pyrite and euhedral Titanium-bearing minerals, probably rutile, are also present throughout, and macroporosity is virtually non-existent.

Laminae are generally horizontal, and range from less than 1 mm apart (Fig. 8A and B) to several centimetres between visible laminae (Fig. 8C). Spacing of laminae is generally irregular, although apparent rhythmicity on a centimetre-scale is present in places throughout unit OSCS-E. Within these silty mudstones are some less-common sandy laminae that display a variety of sedimentary structures. These thin sands are often in the form of very fine-grained lenses or asymmetric starved ripples (Fig. 8C). Flame structures (Fig. 8D) and 'ball and pillow' structures (Fig. 8E) are also present, some having current indicators (for example, oriented, asymmetrical flames, clay drapes, etc.) indicating a west or north-westerly flow direction. These sandier layers never attain thicknesses greater than 2 cm in this lithofacies and are uncommon throughout the Billy Springs Formation. Transitions to other lithofacies are either sharp (Fig. 8F), or more gradual, with internal erosive surfaces and microfaulting occurring at some transitions to the convolute-laminated lithofacies (Fig. 8G). In some locations, planar laminae appear have a rhythmic or cyclical character of thickness variation (Fig. 8H). In these areas, spacing of laminae appears to be regular or rhythmic in their distribution and thickness, so a small section of apparently rhythmic laminae was analysed for the presence of cyclicity in the thickness of laminae. The thicknesses of 524 laminae in a sample were measured and categorized as to whether they were light or dark in colour. Fourier analysis of this set of apparently rhythmic laminae reveals the presence of at least two periods of cyclicity in laminae thickness distribution (Fig. 9). Cycles occur every 64 and 32 laminae primarily, with a smaller, less apparent, cycle occurring approximately every 21 laminae. Although the analysis shows the presence and periodicity of a cycle, it does not specify other information about cycle properties or constituent laminae.

Distribution (C)

Silty mudstones with planar laminae form a significant lithofacies in both the southern and northern sections (Fig. 5). Above the uppermost slumped unit in section OSCS (at *ca* 530 m), Unit OSCS-E is characterized by a thick, continuous section of planar-laminated silty mudstones. In this unit, no slumping, large clasts, or sedimentary structures are present for approximately 450 m of vertical section (*ca* 530 to 980 m). Although exposures are relatively continuous, neither sand-dominated laminae nor thicker sand beds were seen within this interval. In the north, units dominated by planar-laminated mudstones were common, interbedded with convolute-laminated mudstones.

Interpretation and controls on planar laminae (C)

Small grain size, the consistent fine-grained nature of planar-laminated mudstones, and the lack of high-energy sedimentary structures suggests deposition in a low-energy environment with few significant perturbations. Many of the planar-laminated silty mudstones described here most closely resemble muddy contourites or pelagites (e.g. Pickering et al 1989; Shanmugam, 2008; Rebesco et al. 2014); sediments deposited below storm wave base in deeper marine environments. Such deposits can occur on the continental shelf, slope and abyssal plain. However, the proximity, both spatial and stratigraphic, to known shallow-water deposits (for example, shoreface sands in the Bonney Sandstone tens of kilometres to the south) makes it unlikely that sea-levels in the Adelaide Rift Complex reached abyssal depths; previous reconstructions suggest that sediments were deposited on a platform between two landmasses (Preiss, 1990). It is unlikely that water depths reached more than several hundred metres at maximum. Planar-laminated mudstones are thus interpreted to be the product of background sedimentation below storm wave base but close enough to source areas to receive substantial amounts of silt and occasional sands. Intermittent, centimetre-thick beds of very fine-grained sand or silt with current indicators (for example, Fig. 8C to E), as well as the overall abundance of silty laminae, suggest that bottom currents were weak, but were fairly common occurrences, possibly related to storm activity. The lack of infaunal organisms in the Ediacaran accounts for the preservation of micron-scale laminae; analogous deposits from the Phanerozoic commonly include some degree of bioturbation.

The periodicities of 32 and 64 laminae from the analyzed example represent a count of both light (coarser-grained) and dark (finer-grained) layers. In similar analyses on other rhythmically laminated sediments, laminae have been interpreted as comprising a light/dark pair (e.g. Williams, 1988). Thus, a cycle period of 32 laminae in the Billy Springs Formation corresponds to 16 pairs of light and dark layers. In the Elatina Formation elsewhere in the Adelaide Rift Complex, rhythmic sediments are composed of bundles with 11 to 14 laminae each (Williams, 1988). The Reynella Siltstone has cyclic laminae bundles composed of 14 to 15 laminae, each with a lighter sand and darker clay component (Williams, 1990), and the Chambers Bluff Tillite contains bundles with 15 to 25 light-dark pairs (Williams, 1988). The individual light-dark laminae pairs in these sediments are interpreted as being the product of diurnal or semi-diurnal tidal deposition, with bundles ('lamina-cycles') representing lunar fortnightly cycles. The Billy Springs laminae may be interpreted similarly – a cycle of 16 light–dark pairs is the maximum number reported from the Elatina and is not dissimilar to cyclicity reported in these other Neoproterozoic sediments. Laminae in the Billy Springs could therefore be interpreted as diurnal and the cyclicity resulting from neap–spring tidal processes. The larger, stronger cycle of 64 laminae (32 light–dark pairs) may then represent a monthly cycle, as are sometimes seen in both modern environments and in ancient sediments (e.g. Archer, 1991, Kvale et al., 1995). Alternatively, individual laminae may be semi-diurnal, with four laminae deposited per day, leading to 32 light–dark pairs per fortnight, with the secondary cycle representing only the strongest of asymmetrical semidiurnal tides. The smallest cycle of 21 laminae (*ca* 10 light–dark pairs) is not as strong, and does not tie readily to known processes. Given that the data analyzed contain a fair amount of noise, and some error exists in measuring sub-millimetre scale laminae, such conclusions should be taken as speculative, underscoring the need for further research. Other time periods for cycles are possible, but would lead to unreasonably long deposition times for the entire succession.

Similar laminated clastic deposits have been interpreted in the past as the product of seasonal melt-water cycles (Cowan et al., 1999; Eyles & Januszczak, 2004, and references therein), tidal deposits (Mazumder & Arima, 2013; Cowan et al. 1998), or climate-related storm activity (Shanmugam, 1980). Millimetre-scale, fine alternations in grain size similar to those seen here have also been interpreted as the distal ends of muddy turbidite deposits (Stow & Piper, 1984). Some laminae and thin sands have probably been reworked subsequently by weak bottom currents, resulting in the range of unidirectional current features seen on occasion.

Convolute-laminated silty mudstone (Lithofacies *Mcl*) (B)

Description (C)

Lithologically, convolute-laminated silty mudstones are almost identical to planar-laminated silty mudstones. In thin section, both lithofacies show a clay-dominated matrix with abundant silt-sized quartz grains (Fig. 10); very fine to fine-grained sands are also present but uncommon. Like the planar-laminated mudstones, laminae are visible due to differences in silt or quartz content between individual layers, although sub centimetre-scale laminae do not exist in all beds. Larger isolated clasts (cobble to boulder-sized) are rare, but present, within the some convolute-laminated mudstones, especially in the northern section. These are distinguished from more concentrated intervals of larger clasts, which form a different lithofacies and are discussed below.

To compare lithofacies *Mcl* with lithofacies *Pcl*, X-ray diffraction analysis was conducted on two samples from each lithofacies (Fig. 11). Results show that both share a very similar assemblage of detrital grains. Relative abundances can very generally be deduced from peak heights. The primary constituent of both lithofacies is quartz, followed by plagioclase feldspar, carbonates (dolomite and calcite) Chlorite (Chamosite) and Muscovite (including Phengite). Although the exact mineralogical composition and abundance varied between samples, overall lithologies were consistent across the four units analyzed.

Despite these similarities, the nature of bedding and laminae varies substantially between the two lithofacies. Convolute-laminated mudstones display soft-sediment deformation at a range of scales, from cm-scale, tight isoclinal folds (Fig. 12A and B), to broad, gently curving arcs several metres across (Fig. 12C and D). This lithofacies is generally contained within discrete, metre-scale beds, especially in the northern section, but may pinch-out, or, in the southern section, grade laterally into planar-laminated mudstone lithofacies (Fig. 12E and F). Within convolute-laminated units, internal scour or truncation surfaces are sometimes present, indicating that individual units may be composed of a series of multiple erosive, slump-generating events (Fig. 12G). Individual beds cannot be readily distinguished within this lithofacies, and laminae within folds are relatively continuous. Minor sedimentary structures include radial fluid-escape structures (Fig. 12H), which are likely to be related to the highly fluid sediment associated with soft-sediment deformation.

Convolute-laminated beds in the lower part of section OSCS take the form of discontinuous, metre-scale ‘pods’ of silty sediment that weather in relief in comparison to surrounding shales (similar to Fig. 12F). Internally, beds can be seen as containing laminae with a range of deformation styles and scales. In areas with good exposure, convolute beds can be seen to grade laterally into finer-grained, planar-bedded shale units. Elsewhere in OSCS, slumps are more continuous.

Distribution (C)

The first appearance of convolute-laminated sediments is taken here to be the base of the Billy Springs Formation, because lithologies below this point agree with published descriptions of the Wonoka Formation, and the first appearance of significant slumping marks a distinct lithofacies change from units below. Convolute-laminated facies (*Mcl*) are interbedded with planar-laminated lithofacies (*Mpl*) for the lower *ca* 530 m of section OSCS, becoming more continuous toward the top of this interval. For several hundred metres above this distinct marker unit (at *ca* 240 m), discrete convolute beds are sparser, until about 500 m above the base of the formation where the succession of slumped beds terminates with a relatively continuous unit.

The northern measured section also shows a distinct lithofacies change with the underlying Wonoka Formation, at a point which coincides with the formation boundary as previously mapped on the 1 : 63360 map sheet. The uppermost Wonoka Formation in this area is also grey, clay-rich, silty shale, similar to that seen in the southern section. Here (30°11'30.24"S, 139° 1'1.30"E), the formation boundary is marked by a sharp-based contact with a thick (18 m) unit composed entirely of convolute bedded-silty mudstones. Lithofacies *Mcl* occurs throughout most of the rest of the northern section, alternating with lithofacies *Mpl*.

Interpretation (C)

The convolute laminated beds in this lithofacies are interpreted to be the depositional products of submarine slumping, a process distinct from both turbidity currents and debris flows (Strachan, 2008; Stow & Mayall, 2000). Unlike these other mass flow processes, slumping results in a cohesive deposit that maintains internal structure while deforming it, in contrast to other mass flow deposits in which traces of original stratification are destroyed by shearing, mixing and dilution (Strachan, 2008). Thus, slumps and their products typically represent an earlier or less mature stage in mass movements (Stow et al, 1986). The variety of soft-sediment fold morphologies seen in these beds may be related to the transport distance of each slump bed; laminae would become progressively deformed with further transport. The presence of larger, isolated clasts within this lithofacies is discussed below.

Lithofacies association 1: Planar-laminated and convolute-laminated mudstones (B)

Occurrence

Planar-laminated and convolute-laminated lithofacies commonly occur in close proximity throughout both sections. In OSCN, this lithofacies association occurs in the northern section as alternating, discrete beds that are composed entirely of one lithofacies or the other (OSCN 0 to 158 m from the base of the section), each several metres thick. Boundaries are generally sharp, but in at least one instance the degree of slumping decreases upward, eventually transitioning into planar laminae (parts of this transition can be seen in Fig. 8G). In the southern section, convolute-laminated beds form both continuous and discontinuous beds within larger packages of planar-laminated mudstone, with discontinuous beds laterally adjacent to lithofacies *Mpl*. In section OSCN, unit F2, a convolute-laminated unit, gradually becomes thinner and appears to pinch out to the south-east over the course of several tens of metres of lateral exposure. Elsewhere along the same section, creek meander bends allow the same stratigraphic interval to be viewed several hundred metres apart; in these sections, the same sequence of slump and planar units does not repeat (for example, Fig. 5). This suggests that these units are not laterally continuous throughout the area, and that the specific arrangement and thicknesses of units would vary in other exposures.

Interpretation (C)

The compositional similarity between planar-laminated and convolute-laminated lithofacies suggests that the convolute-laminated deposits were initially deposited as planar-laminated muds, and then deformed and re-transported by slumping. Although the distance over which slumps can travel before flow transformation into turbidity currents is dependent on a number of factors (gradient, sediment composition, etc.), the lack of other, more mature types of mass flow deposits within this facies association also suggests that this lithofacies is relatively close to its origin.

In section OSCS, discontinuous slump beds several metres across can be seen laterally adjacent to planar-laminated mudstones (Fig. 12E and F). This also is indicative of an intrabasinal, proximal origin for these features; slumping in these areas was taking place on a relatively small scale. This exact arrangement of slump bodies at this scale has not been previously reported, although mass transport deposits, including slumps and debris flows, are commonly part of minibasin fill (e.g. Winker, 1996; Beaubouef et al., 2003; Beaubouef & Friedman, 2000; Olsen & Damuth, 2009). Jackson (2012), for instance, records a large number of discontinuous slide blocks (which may be slump bodies similar to those described here) within a single minibasin, most at a scale of tens of metres to *ca* 300 m across. The abundance of planar-laminated lithofacies (with no slump deposits for hundreds of metres) in the upper two-thirds of the measured section also indicates a relatively stable environment for parts of the Billy Springs interval studied here. The active movement of nearby diapirs and associated subsidence may provide a trigger for slump movement and generation of the convolute-laminated lithofacies. Slope failure and mass transport of sediments are often associated with minibasins, and have been attributed to slope instability resulting from the movement of nearby salt bodies (Giles & Lawton, 2002; Jackson, 2012). Given the common occurrence of slumping and internal lithological consistency of sediments in the sections described here, this intrabasinal triggering is the preferred interpretation for the Billy Springs slump deposits. However, Olsen & Damuth (2009) relate mass transport complexes to external climate cycles, and Aschoff & Giles (2005) interpret some minibasin conglomerates as tsunami deposits; thus, external factors are also known to influence intrabasinal sediment transport.

Matrix-supported diamictite (Lithofacies *Dms*) (B)

Description (C)

Intervals where large clasts are more concentrated (Fig. 13A) are considered diamictites, because the term does not carry a genetic implication, and form lithofacies *Dms*. Even in these intervals (which lack sharp boundaries), clast abundance is generally sparse. Unlike larger clasts found isolated within convolute-laminated mudstones (Fig. 13B and C), lithofacies *Dms* is characterized by an abundance of clasts within a small stratigraphic interval. Large isolated clasts elsewhere in the measured sections are not considered a part of this lithofacies, because they do not occur in dense concentrations.

The composition of large clast assemblages (i.e. all grains larger than sand) falls into two categories: monomictic–intraformational and polymictic. Monomictic clast assemblages are generally composed of silty mudstone that has a very similar lithological composition as the surrounding planar or convolute-laminated sediment. These types of clasts may be found in isolation as part of lithofacies *Mcl*, or in discontinuous beds where they form dense, non-oriented concentrations as part of lithofacies *Dms* (Fig. 13D and E).

The composition of polymictic clast assemblages is entirely different. In these intervals, especially in section OSCS, clasts with 6 to 10 cm diameters were most common. The primary 'boulder bed' (as originally described by Coats & Blissett, 1971) is found in the southern section (Unit OSCS-A) and contains clasts composed of carbonates, white and black chert, quartz and mudstone. The lower section of Unit OSCN-P contains a similar clast assemblage, in addition to at least one large clast of vesicular basalt (Fig. 13F). Within these intervals, silt and mud laminae can sometimes be seen to warp and deform around the clasts on both the top and bottom (Fig. 13D and G). In other instances, such deformed laminae are not immediately obvious (Fig. 13H).

Thin sections and QEMSCAN images reveal a range of smaller clasts in addition to the cobbles and boulders visible in outcrop. Observed clasts include well-rounded coarse quartz sand (Fig. 14A), dolomite composed of euhedral rhombic crystals (Fig. 14B), sandy mudstone (Fig. 14C), coated carbonate grains (Fig. 14D), angular chert fragments (Fig. 14E) and micritic carbonate (Fig. 14F).

Clay-sized particles, which could not be definitively identified through traditional petrography, were identified through QEMSCAN and tied to thin sections. Background matrix is composed primarily of quartz, clays, and micas, not dissimilar to that seen in planar-laminated mudstones (Fig. 7). Thin laminae can be seen within the matrix, and laminae are deformed around larger clasts, with clays and micas more common near clast margins (Fig.

15A). The largest clasts in the QEMSCAN sample were well-rounded, equant carbonates. Carbonate clast interiors ranged from micritic dolomite (Fig. 15B), to dolomite rhombs with calcite rims and sparse matrix with silica-filled pores (Fig. 15C), to sutured, euhedral Dolomite rhombs (Fig. 15D; same clast as in Fig. 14B) and microcrystalline calcite (Fig. 15E). Detailed view of the clastic matrix (Fig. 15F) shows iron oxides (goethite), calcite-filled fractures, and bimodal distribution of quartz grains.

Distribution (C)

Concentrated intervals of larger clasts, sized from less than one to tens of centimetres, were observed within the mudstone matrix in some areas. In section OSCS, anomalous clasts are most abundant within an interval several metres thick – the 'boulder bed' or breccia described by previous workers (e.g. Campana et al., 1961; Coats and Blissett, 1971). Outsized clasts are present but rare outside of this unit, and are not seen in OSCS above 530 m (Fig. 2). In the northern section, the only interval of more abundant clasts seen in that section was a relatively thin portion of unit OSCN-P.

Lithofacies association: Diamictites, outsized clasts and convolute-laminated mudstones (B)

Occurrence (C)

Although diamictites are considered to be a separate lithofacies from isolated outsized clasts, they are both associated with lithofacies *Pcl* and are discussed here together. In no instances are exotic clasts seen in planar-laminated lithofacies; thus, it is most likely that this unclear instance follows the same pattern. Both diamictic intervals and isolated exotic stones are found exclusively in convolute-laminated (slumped) mudstones, although it should be noted that, in bed OSCN-P, the surrounding context of the clast-bearing interval was unclear due to exposure. Although Jenkins (2011) notes the presence of exotic clasts (‘dropstones’) in both planar-laminated and convolute-laminated mudstones in the same section studied here, clasts were not observed in planar-laminated or sandy sediments. A thorough investigation of outcrop in the vicinity of the measured sections showed only the association between exotic clasts and convoluted laminae. Intraformational mudstone clast assemblages are also exclusively associated with convolute-laminated mudstones, although a different process is thought to be responsible for their emplacement.

Interpretation: Sedimentation mechanisms and possible glacial influence (C)

Isolated exotic clasts and diamictites in the Billy Springs Formation have previously been interpreted as being the product of ice-rafted debris associated with a nearby glacier (e.g. Dibona, 1991). These interpretations are predicated on the presence of large extrabasinal clasts within silty mudstones. The association between slumped units, outsized clasts and diamictites is important in interpreting the process behind their emplacement; this association suggests that the two are related in their modes of formation.

In cases where larger clasts contained within slump structures are composed of the same lithology as the surrounding matrix (for example, Fig. 13D and E), there is likely to be a genetic link between slumping and clast generation. These types of concentrations are generally uncommon throughout the sections measured, and are interpreted here as having formed through autobrecciation of semi-consolidated sediment as slumping progresses and becomes increasingly convolute. Reid (1992) draws a similar conclusion in the diamictic intervals in Mt Freeling, although this author attributes to clast generation to structural rather than synsedimentary folding. In the section described here, it is clear that folding occurred prior to lithification and that sediment deformation is a product of redeposition.

In the interpretation by Jenkins (2011), slumping associated with exotic clasts may be the result of ice blocks overloaded with detritus which sank to the bottom and deformed the existing planar-laminated sediment or, alternatively, from icebergs deforming the seafloor and depositing entrained debris whilst initiating slumps. However, interaction of ice with the seafloor is known to produce large, straight furrows and gouges with ridges (Weeks, 2010) unlike the slumped beds seen here.

Although glacial processes are able to explain the presence of large, hydrodynamically out of place exotics within much finer-grained sediment, the presence of such clasts can also be explained by other processes which do not require glacial influence to operate. Eyles & Janusczak (2004) note several instances where diamictic lithofacies are probably the result of mass flow-deposits rather than glacigenic sediments. These authors also provide evidence that lonestones are also a common occurrence within otherwise fine-grained strata, for example, in Canada, Namibia and Virginia, wherein large clasts are transported downslope by turbidity currents or poorly sorted mass flows. Postma et al. (1988) also describe mechanisms where isolated boulders can be emplaced within turbidites. Several occurrences of previously described 'glacial dropstones' have thus been reinterpreted as having a non-glacial origin. While these examples are not identical to those seen in Billy Springs in that they are deposited by turbulent flow rather than slump processes, they demonstrate that there are numerous examples of large clasts having been deposited in a dominantly fine-grained environment by non-glacial, processes.

The lack of definitive glacial indicators such as striated and faceted clasts, the strong association of clasts with slumped beds, the significant lack of these clasts in planar-laminated facies and the limited stratigraphic and spatial extent of diamictite deposits all provide evidence against a glacial interpretation. In addition, as clasts are very sparse overall and do not occur above 300 m from the base of the southern section, such a glaciation would be very limited in both time and space. Glacial diamictites elsewhere in the basin (the Sturtian and Marinoan events) are much thicker (up to two kilometres thick in the Sturtian; see Preiss, 1987, fig. 52) and are regarded as 'very reliable' by Hoffman & Schrag (2002), in contrast to the ambiguous features seen in the Billy Springs Formation.

The source of exotic clasts in Billy Springs may then be related to the salt-tectonic environment of the Adelaide Rift Complex. There are numerous examples in the basin of salt diapirs, now exposed in cross-section as dolomitic breccia, having influenced topography or being subaerially exposed during the late Neoproterozoic. Diapir-generated topographic highs are often associated with conglomerates composed of shed diapiric detritus as well as thinning and onlap of formations in the Wilpena Group and elsewhere (e.g. Dyson 2004a, Lemon, 2000). Diapir-generated conglomerates elsewhere in the succession are composed of extrabasinal clasts brought upward from deeper in the basin, often from the rift sediments of the Callanna Group, and include many of the general lithologies seen here (Preiss, 1987).

Tabular-bedded sandstone (Lithofacies *Stb*) (B)

Description (C)

Sand beds are generally decimetre-scale in thickness and separated by slightly thicker mudstone intervals of lithofacies *Mpl*. Sands are fine-grained, often with rippled or undulatory tops and internal ripple cross-lamination. Sand beds are have no obvious lateral bed thickness variation at outcrop scale (Fig. 16), the bases are generally flat or gently undulatory (Fig. 16A) and the tops often contain asymmetrical ripples (Fig. 16B). Internally, sands may be massive, planar-laminated, ripple cross-laminated, hummocky cross-stratified, (for example, Fig. 16C), or some combination of these, and also may contain tepee-shaped water escape structures (Fig. 16D; cf. van Loon 2009, fig 25C). Fining-upward beds (Fig. 16E) and planar to ripple-laminated transitions (Fig. 16F) are suggestive of partial Bouma sequences (B to E divisions). In OSC-S, tabular sand beds appear in relatively isolated groups of three or four beds (for example, Fig. 16A and B), or in larger stacked sequences separated by slightly thicker intervals of planar-laminated silty mudstone (OSC-N; Fig. 16G). Mudstone intervals between sand beds do not appear to have any vertical trend in distribution or spacing.

Thin section analysis revealed that even in the lowermost, sandiest parts of these beds, clay was still present, and grain size was relatively small (Fig. 17A and B). Basal sand beds were dominated by very fine-grained sand and silt, and included a high proportion of heavy minerals (Fig. 17B and C). At the highest stratigraphic point reached in section OSCS, a thicker bed of quartzose sand was poorly exposed on hilltops (unit OSCS-H) that was either massive or showed faint cross stratification. Due to weathering, true thickness of this bed could not be determined, but exposures revealed a bright white, clean sandstone with little or no clay content, confirmed later by petrography to consist of almost entirely upper very fine-grained to lower fine-grained quartz sand (Fig. 17D and E). Quartz grains were dominantly monocrystalline, and sands included a smaller proportion of heavy minerals than that seen in beds below (Fig. 17F).

Distribution (C)

In section OSCS, this lithofacies is present approximately 980 stratigraphic metres from the base of the formation as very fine to fine-grained sand beds several centimetres thick within the planar-laminated mudstones (Fig. 8C to E). Above these beds, a vertical section exposed for approximately 50 m was reconnoitred for any additional sands, but none were seen, with planar-laminated mudstones again dominant. The thicker quartz arenite bed or beds in section OSCS constitute the stratigraphically highest unit measured.

In section OSCN, outcrop exposure becomes less continuous near the top, and thickness measurements are approximate. In the uppermost two units observed (OSCN-N and OSCN-P), tabular, centimetre to decimetre-scale sandy beds are present and weather in relief. These beds have a clear fining-upward grain size and are stacked for several tens of metres to the uppermost point measured in OSCN. It is not possible to directly correlate individual beds in the northern section to specific beds or units in OSCS, although this lithofacies occurs at the tops of both sections.

Interpretation of tabular-bedded sandstones (C)

Interbedded sandstone–mudstone lithofacies are interpreted as turbidites based on the observed sedimentological features within beds, including fining-upward grain sizes, sharp-based sands and partial Bouma sequences. Compared with the other lithofacies, the presence of these coarser-grained beds and sediments deposited by turbulent flow implies a change in both the depositional process and the likely proximity to source areas. Because slumped sediments are still mud-dominated and do not show a marked increase in sand content, it is more likely that they are formed by deformation of local, intrabasinal sediment. Although slump and turbidite processes can generally be seen as part of the same sediment gravity flow continuum, the lithological, geometric and thickness differences between these two lithofacies implies that these lithofacies are not necessarily genetically related. Turbidites, being dominated by sands, probably have a different source and may be brought in by gravity flows from outside the immediate area of deposition.

The distribution of these turbidites has implications for the sequence stratigraphic interpretation of the Billy Springs Formation. As sandy turbidite lithofacies are limited only to intervals stratigraphically higher in the section, the Billy Springs Formation is interpreted to be progressively shallowing upward as sand-rich sediments prograde out over the deeper water muds. The formation may represent the distal portion of a highstand systems tract, with the turbidite sands seen near the top being the earliest prodelta deposits in the sequence to be deposited far into the basin, although without clear correlations to other formations, such an interpretation is not conclusive. The time-equivalent Bonney Sandstone has been interpreted elsewhere as having been deposited in an interval of relatively falling sea-level during a highstand systems tract (sequence M4.3 of Preiss, 1999, and 4.4 of Preiss, 2000) that terminates with an erosional surface at the base of either the Chace or Ediacara members within the Rawnsley Quartzite (Preiss, 1987, Preiss, 1999, Gehling 2000). The Billy Springs Formation sediments consist of thick fine-grained lithologies that are likely to be deposited in deeper water than much of the rest of the Wilpena Group, and show an overall, large-scale coarsening-up profile. Such profiles are characteristic of late highstand, where sedimentation rate surpasses the rate of sea-level rise, and accommodation space begins to fill during normal regression (Posamentier & Allen, 1999). Reid (1992) also interprets uppermost sandier beds to represent the incursion of the Pound Subgroup; an interpretation which generally agrees with the observations and interpretations herein, although this study cannot definitively assess exactly where in the upper Wilpena Group these sandy turbidites originate from.

DISCUSSION AND SIGNIFICANCE (A)

A glacial source for extrabasinal clasts? (B)

The hypothesis of a ‘Billy Springs glaciation’ in the late Ediacaran requires the support of several lines of evidence to be widely accepted. Thus far, the only evidence lies in the presence of extrabasinal clasts within relatively narrow intervals. Potentially glacial sediments would be expected to be related to known glacial intervals in the surrounding area and beyond. Given the established low latitude for the South Australia during this time (Li et al., 2008), a Billy Springs glaciation would need to either be global in scale, or be due to extensive high-altitude glaciers reaching sea-level. The well-known Sturtian and Marinoan glacial episodes are present stratigraphically below the Billy Springs Formation by hundreds or thousands of metres. Therefore, any potential glacial debris in the Billy Springs Formation likely post-dates these events by millions of years. The best candidate for a correlative interval in Australia that may show glacial evidence is the Egan Formation in the Kimberley Region of Western Australia, which contains diamictites and has been interpreted to post-date the Elatina/Marinoan glaciation (Corkeron & George, 2001; Bao et al. 2012). Grey & Corkeron (1998) tie the Egan interval to the Wonoka Formation on the basis of stromatolite biostratigraphy; thus, a brief glacial event corresponding to the Egan interval cannot therefore be ruled out for the time of Billy Springs/Wonoka deposition, although it should be noted that there are no glacial deposits elsewhere in either the Wonoka Formation or in the equivalent Julie Formation in the Amadeus Basin. In addition, Coats & Preiss (1980) and several older publications interpret the Egan sediment as Marinoan and equivalent to the Elatina Formation rather than the Wonoka Formation.

The only other widespread Ediacaran glaciation with significant support is the Gaskiers event, known initially from Canadian deposits. Unlike the Sturtian and Marinoan intervals, which are global in scale, the Gaskiers glacial interval is found primarily in areas reconstructed to be in high-latitudes at the time of deposition (Hoffman & Li, 2009). The relatively short duration of the event and the lack of cap carbonates are inconsistent with a global glaciation (Li et al., 2013), making it unlikely that the low-latitude Adelaide Rift Complex would be ice-covered. The glacial interpretations of other low-latitude diamictite-bearing formations associated with the Gaskiers glaciation have also been called into question (e.g. Direen & Jago, 2008; Hoffman et al., 2009; Carto & Eyles, 2012). Most authors place the Gaskiers event at around 580 Ma (Bowring et al, 2003; Hoffman & Li, 2009; Li et al., 2013). The timing also presents an issue; most time scales place the maximum age of the Bonney Sandstone (and, by extension, the middle Billy Springs Formation; Pell et al., 1993) almost 30 Myr later (Preiss, 2000). Jenkins (2011) acknowledges that the Gaskiers Event may be too early to correlate to the Billy Springs Formation. Thus, it is unlikely that this event resulted in, or was contemporaneous with, deposition of parts of the Billy Springs Formation. Hebert et al (2012) and a few other authors (e.g. Chumakov, 2009) hypothesize the existence of a post-Gaskiers glaciation, although evidence is not widespread. The glacial-origin scenario is therefore considered less likely than the more parsimonious suggestion of a non-glacial depositional mechanism.

Umberatana Syncline as a Salt-Withdrawal Minibasin (B)

The structural complexity of the basin fill can make it difficult to recognize syn-sedimentary subsidence and faulting; however, careful examination of thickness variations, relationships to diapir bodies and lateral facies changes show that much deformation occurred during the deposition of the basin fill and prior to the Delamerian event (Dalgarno &

Johnson, 1968; Coats, 1973; Lemon, 1985; Rowan & Vendeville, 2006). The majority of this deformation can be attributed to the upward growth of salt diapirs and associated subsidence from mobilization and withdrawal of an underlying bedded salt layer (Hearon et al., 2014). Numerous (>100) diapir bodies are now exposed throughout the Adelaide Rift Complex over an area of approximately 50,000 km^2, and much of the current structure in the Flinders Ranges is likely due to pre-Delamerian halokinesis instead of structural compression, especially in the northern part of the basin discussed here (Fig. 19) (Rowan & Vendeville, 2006). Like the Umberatana syncline, many structures originate or terminate at diapirs (Curtis & Jenkins, 1991; Dyson, 2001; Rowan & Vendeville, 2006). Previous studies that attribute folding only to tectonic processes (e.g. Paul et al., 1999) ignore the thickness changes in these units, which are unambiguous evidence of a syn-depositional origin. Clear indications of syn-sedimentary diapirism and subsidence are found as far back as the Sturtian glacials in the Umberatana Group, continue into the Cambrian, and are present in all formations in between (Coats, 1973, Table 2). Sediments adjacent to diapirs often contain conglomeratic bands within otherwise homogenous, finer-grained formations or, in the Enorama Shale, reef development around the emergent diapir margin (Lemon, 2000). Many diapir bodies show relationships with adjacent sediments that indicate that they were exposed or formed topographic relief at the sediment-water interface, with some diapiric highs possibly becoming emergent and forming subaerial islands (Dalgarno & Johnson, 1968; Plummer, 1978; Lemon, 2000).

Sediments that are generally correlative to the Billy Springs Formation also often show indications of minibasin formation near diapirs. Clearly defined onlap or conglomeratic facies are documented in the upper Wilpena Group near the Oratunga, Pinda, Patawarta, Mount Frome, Wirrealpa and Beltana diapirs (Dalgarno & Johnson, 1968; Lemon, 1985;

Reilly, 2001; Dyson, 2004a; Kernan et al., 2012; Collie & Giles, 2001; Dyson, 2004, Hearon et al., 2015), most of which are less than 100 km from the Billy Springs Formation. Such relationships clearly indicate that active salt movement and subsidence was ongoing throughout the basin during the time of Bonney and Wonoka deposition and, by extension, during the time of Billy Springs deposition as well. The Umberatana Syncline has specifically been interpreted previously as a salt-withdrawal minibasin (Rowan & Vendeville, 2006), with its syncline axis originating from the Lyndhurst diapir *ca* 40 km to the west. Other diapir bodies occur in close proximity as well, with the closest only 4 km from the sections described here. The Burr diapir, the largest in the basin in terms of outcrop area (Fig.19A; Coats, 1973), is less than 20 km to the west. The size and shape of the Umberatana syncline also conforms to minibasins seen today in the Gulf of Mexico (Bryant et al., 1990; Bouma & Bryant, 1995) and the Santos basin (Jackson, 2012), where minibasins form sub-circular depressions with diameters of 10 to 20 km separated at depth by irregular salt piercements (Fig. 19C). Later erosion, however, prevents precise reconstruction of halokinetic sequences in the Umberatana area, because the contact between the upper Ediacaran sediments and the diapir body is not preserved.

Sedimentation in the Umberatana syncline shows similarities with other documented intraslope or lower shelf minibasins. Alternating intervals of pelagic deposition and mass-transport complexes are also seen in the Gulf of Mexico (e.g. Madof et al., 2009), although at a scale much larger than that seen here and visible on seismic data. In core from the subsurface of the Gulf of Mexico, minibasins in modern and Pleistocene sediments have also been described as being partially filled by homogenous and finely-laminated muds (Mallarino et al., 2006). Section OSC-S bears some degree of similarity to that observed by Shultz & Hubbard (2005), who describe ponded turbidites increasing in frequency upward in an intraslope minibasin from Chile, as well as slumps, slides and debris flows. Likewise, the fine-grained nature of the Umberatana minibasin resembles conceptual models by Banham & Mountney (2013a; see Fig. 13F) as occurring in high subsidence, low sediment supply continental environments, where lacustrine settings would dominate. Thus, these sediments add further evidence to a growing compilation of recurring features in these environments across space and time. However, The Umberatana Syncline is also unique amongst outcropping minibasins in that it is finer-grained, less variable in lithology, and was formed in a deeper water environment than many others described in the literature (see Table 1). The minibasin described in this study, therefore, represents an end-member in the spectrum of depositional settings in which minibasins form. As such, it more closely matches the environment of deposition of many of the actively producing hydrocarbon plays, which are common in deep-water, offshore settings.

The sections described here are dominated by hundreds of metres of silty mudstone (Fig. 5), interpreted as having been deposited in a shelf or slope environment. The lower Billy Springs Formation thus provides an example of a minibasin wherein much of the basin fill is lacking in sediments which would have the potential to be hydrocarbon reservoirs. The rarity of sand-dominant sediments in the Umberatana minibasin interior implies that either: (i) no coarser sediments were available from the source; (ii) subsidence was relatively slow, forming only a low gradient which did not favor the trapping of sands; or (iii) coarser sediment depocentres are elsewhere in the basin and sands have laterally bypassed the Umberatana area (sediment bypass of minibasins is described by Mallarino et al., 2006). Turbidites and slumping are often characteristic features of minibasins (Table 1). Minibasin sedimentation patterns are often related to halokinetic control (e.g. Giles & Lawton, 2002); in the Umberatana syncline, slumping is likely intrabasinal, and the frequency of slumped intervals suggests that it may be halokinetically triggered. However, the overall sequence stratigraphic setting and depositional environment may be more dominant in controlling lithologies, because the coarsening-upward succession of sediments described here fits better with a larger change in sediment supply.

Relevance to Ediacaran Metazoan Assemblage (B)

This study provides further environmental and stratigraphic context for the Ediacaran fossil fauna preserved in the Ediacara Member of the Rawnsley Quartzite (for background, see Gehling, 2000; Narbonne, 2005). It is likely that the primary fossil-bearing strata directly overlie the Billy Springs Formation sediments discussed here as reported by Reid (1992), with fossils occurring north of the study area. Pound Subgroup sands atop the Billy Springs Formation are likely to be part of the continued progradation of coarser sediments over those seen in the Umberatana area, and suggest a widespread shallowing-upward sequence across the basin in upper Wilpena Group time. The presence of a definitively marine, shelf/slope facies in the immediately subjacent sediments should also influence palaeogeographic reconstructions of the area. Such a depocentre implies an overall deepening of the basin, and possibly an oceanic connection to the north-west of the central basin axis, which would probably have persisted to some degree during the time of Rawnsley deposition. Future studies reconstructing regional palaeoenvironments during the time of metazoan colonization may benefit from this inclusion. Given the widespread indications of syn-sedimentary diapirism during Pound Subgroup time, more work should also be done to better understand the effects of diapir-induced topography on the distribution of fossils and the lithofacies in which they are found.

CONCLUSIONS (A)

Sediments of the Billy Springs Formation, described in detail for the first time here, show a range of features (fine-grained laminated sediments, slump structures and turbidite deposits) consistent with deposition within a deep water intra-shelf or intra-slope minibasin. Although minibasins are known from several outcrops elsewhere in Australia and around the world, few have been studied from a sedimentological perspective, and the Umberatana minibasin is a unique exposure in terms of its sedimentary character and palaeogeographic setting. Lithofacies within the basin reflect background pelagic deposition, intrabasinal slumping and progradation of turbidite sands into the basin. Rhythmically laminated facies may be the product of changing depositional energy related to short-term cycles, possibly tidal. Association between diamictites and slump structures suggests that these lithofacies were emplaced by the same depositional processes. Large extrabasinal clasts are probably sourced from nearby salt diapirs, which are present throughout the basin and are known elsewhere to shed conglomerates. Clasts are likely to have originated from deeper in the basin, and were subsequently brought to the surface by nearby salt diapirs and re-deposited. Previous interpretations that clasts are glacial in origin are inconsistent with the timing and extent of known glacial intervals, except potentially for the Egan Glacials of north-western Australia, for which timing is poorly constrained; sediments are probably too young to correlate to the Gaskiers event. Because deepwater sediments are uncommon in the Adelaide Rift Complex, the presence of a shelf or slope environment within the northern Flinders Ranges also has important implications for the palaeogeography of the larger basin. The northern Adelaide Rift Complex, therefore, may have been a more complex depositional system than previously believed, and is an excellent outcrop analogue for similar depositional settings in the geological record.

ACKNOWLEDGEMENTS (A)

This research is supported in part by the Nancy Setzer Murray Memorial Grant from AAPG Foundation, a part of AAPG Grants-In-Aid program and the University of Adelaide, who supported this research through an International Postgraduate Research Scholarship. The authors would like to thank Bob Dalgarno, Jim Gehling and Wolfgang Preiss for helpful discussions throughout this process, as well as the Reservoir Analogues Research Group (RARG) at the Australian School of Petroleum, University of Adelaide. We thank James Manual at the Ian Wark Research Institute at the University of South Australia who performed QEMSCAN analysis, and Melissa Craig, who assisted with Fourier analysis. Thanks are also due to Umberatana Station owners Chris and Jenny Mahoney, who graciously provided land access, and Claudia Valenti, who proved to be an invaluable assistant during field work. We acknowledge the traditional owners of the lands on which this research was conducted. This paper forms record number 333 of the Centre for Tectonics, Resources, and Exploration at the University of Adelaide.

LIST OF TABLES (A)

Table 1: Summary of salt-withdrawal minibasin studies in published literature, including only those where some component of sedimentology has been described. Studies are arranged by the dominant depositional environment in which the minibasin formed, although several examples encompass many different depositional settings.

Table 2: Comprehensive list and summary of previous investigations of the Billy Springs Formation that discuss sedimentology or stratigraphy.

Table 3: Brief description of stratigraphic units, measured section OSCS. Corresponds to Units in Fig. 5A.

Table 4: Brief description of stratigraphic units, measured section OSCN. Corresponds to listed units on stratigraphic column in Fig. 5B

LIST OF FIGURES (A)

Fig. 1: Map of Australia showing major cratonic provinces, selected sedimentary basins and Centralian Superbasin.

Fig. 2: Locator map showing Adelaide Basin and field sites in relation to surrounding basins and cratonic provinces. The Officer Basin is of a similar age to the Adelaide Basin and the Warburton Basin is Cambro-Ordovician in age.

Fig. 3: Generalized lithostratigraphy of the Adelaide Rift Complex, Wilpena Group and Pound Subgroup.

Fig. 4: Geological map of the field area, from the GSSA Copley and Maree 1 : 250,000 map sheets published in 1973 and 2012, respectively. Modified from Coats (1973).

Fig.5: Stratigraphic sections measured in this study. (A) OSCS and (B) OSCN. Both sections were measured in Old Station Creek (see locations in Fig. 4). Sections were measured from the base of the Billy Springs Formation and are thus potentially equivalent. Section OSCN is also shown at an expanded scale, and includes the shorter, repeat section (approximately 250 distant) seen in creek meanders that illustrates the discontinuous nature of convolute-laminated and planar-laminated units in this area.

Fig.6: Planar-laminated mudstone in thin-section. (A) In more rhythmic intervals, individual laminae have a stronger compositional difference in the amount of quartz silts, which can be seen in thin section. (B) Typical matrix of planar-laminated silty mudstones, wherein individual laminae are very faint with respect to sediment composition.

Fig. 7: QEMSCAN images of planar-laminated lithofacies, Unit OSCS-G. (A) Wide-field view of typical planar-laminated interval, showing mineralogical differences in laminae

related to alternation between quartz and clay percentage. (B) Same sample as (A), showing preservation of micron-scale laminae. (C) Quartz-dominated layer, showing sediment composition including euhedral Rutile (?) crystals.

Fig. 8: Planar-laminated mudstone lithofacies: macroscopic character and sedimentary structures. (A) Representative nature of planar laminae in OSCS-E, showing planar laminae. (B) Typical nature of planar-laminated lithofacies in most outcrops, lacking significant sand laminae or readily identifiable rhythmicity, unit OSCN-L. (C) Very fine-grained sand laminae, lenses and starved ripples in silty mudstone matrix, OSCN-D. (D) Ball and pillow and flame structures, unit OSCN-B. Darker laminae forming re-entrants are composed of slightly higher silt content than surrounding well-indurated mudstones. (E) Sandy laminae and clay-draped ball and pillow structures, OSCN-H, showing generally north-western flow direction. Inset: continuous nature of same centimetre-scale beds/laminae. (F) Sharp boundary between OSCN units A and B. Planar laminae can be seen to drape over undulatory contact (contact noted by arrows). (G) Synsedimentary microfaulting and scour, at the transition between units OSCN-L and OSCN-M. Beds gradually become increasing contorted upward. Minor scours/faulting in white dashed line. (H) Mid-unit OSCS-E, showing rhythmic nature of planar laminae in certain intervals.

Fig. 9: Rhythmite histogram and analysis. (A) Thickness of each laminae within a preselected interval similar to that seen in Fig. 8H. (B) Fourier Analysis plot, showing magnitude of Fourier transform versus frequency, assuming one time unit per laminae. (C) Same data as in (B), with frequency converted to laminae number.

Fig. 10: Convolute-laminated lithofacies in thin-section. This lithofacies is often indistinguishable from planar-laminated mudstone lithofacies petrographically.

Fig. 11: X-ray diffraction analysis of silty mudstones from planar-laminated and convolute-laminated lithofacies. Coloured bars in grey-shaded stick chart denote known peaks for each

mineral, and correspond to highlighted peaks in sample. Listed order of mineralogy does not imply differences in quantitative abundance.

Fig. 12: Convolute laminated silty mudstone lithofacies: outcrop photos. (A) and (B) Decimetre to metre-scale beds containing highly convolute laminae, unit OSCN-I. (C) and (D) Broad, irregular folds in units OSCN-G and OSCN-I, respectively. Such folds occur in conjunction with smaller-scale folds as seen in (A) and (B). In (C) the field notebook is 15 cm high. (E) and (F) Discontinuous nature of convolute-laminated lithofacies in OSCS: (E), showing individual slump body within overall planar-laminated mudstone; and (F), showing slump bodies weathering in relief along strike to OSCN-A. (G) Distinct reactivation or scour surface with downlapping laminae, near base of unit OSCN-M. (H) Radial fluid escape structure in OSCN-C. Note the sharp boundaries, distinct surface and infilling of overlying laminae into subvertical pipes.

Fig. 13: Diamictites, boulders and exotic clasts found in the Billy Springs Formation. (A) Upper OSCS-A, one of the few intervals with sufficient clast density to be classified as a diamictite. Visible are black and white cherts and reddish-brown-weathering limestone/dolomite clasts. (B) Well-rounded mudstone boulder in OSCN-C. (C) Well-rounded carbonate cobble in OSCN-M. (D) Autobrecciated slump bed, with contorted clasts of the same or similar lithology to surrounding matrix. (E) Discrete clast-bearing unit between convolute-laminated beds, OSCN-M. (F) Cobble of vesicular basalt found in lower OSCN-P. (G) Clast within convolute-laminae, showing distortion of laminae around clasts. (H) Large, partially dissolved carbonate clasts, as well as smaller sand and granule sized particles in mudstone matrix.

Fig. 14: Wide range of exotic clasts seen in two 2” x 3” thin sections from upper unit OSCS-A. All samples oriented correctly except (C), found as a float block. (A) Well-rounded fine- to upper coarse-grained monocrystalline quartz sand within a matrix of silty/sandy mudstone.

(B) Large clast of well-packed crystals of rhombohedral carbonate (mineralogy from Qemscan; presented in Fig. 15). Euhedral zoning visible in crystal interiors. Between crystals is an isotropic groundmass of undetermined composition. (C) Millimetre-scale clast in silty mudstone matrix, composed of very-fine to fine-grained sand within a dark, clay-rich matrix. (D) Interior of large clast containing coated grains of crystalline carbonate. Rounding and micritic rims of grains predate cementation and indicate extended weathering of grain cores prior to coating. (E) Composite image showing range of clast lithologies on sub-centimetre scale: microcrystalline quartz (chert), micrite, cryptocrystalline carbonate and sand. Note the variable silt content of matrix. (F) Micrite-dominated carbonate clast deforming grain alignments in silty mudstone matrix.

Fig. 15: QEMSCAN images showing detailed mineralogy of sample in unit OSCS-H, diamictite lithofacies. (A) Wide-field view showing several millimetre-scale, well-rounded carbonate clasts in a clastic matrix dominated by quartz, mica and clays. (B) and (C) detailed views of interior of carbonate clasts seen in (A): (B) dominated by microcrystalline dolomite; and (C) by a mixture of dolomite/calcite crystals with silica in interstices. (D) Detailed view of individual clast composed of euhedral, rhombic dolomite crystals with calcite-rich alteration rims and interior zonation. Clastic matrix external to clast is composed predominantly of quartz, feldspars and micas. (E) Micritic calcite clast boundary, from elsewhere in the same sample. (F) Detail of matrix, showing large, well-rounded quartz sand grain that differs texturally from background matrix, as well as (possibly authigenic) goethite, chlorite and fracture-filling calcite.

Fig 16: Interbedded sandstone-mudstone lithofacies. (A) Centimetre-scale sand beds atop 700 m of planar-laminated mudstone, OSCS-F. (B) Grouped, tabular centimetre-scale beds with asymmetrically rippled tops, OSCN-P. (C) Internally-ripple-laminated and hummocky cross-stratified sand bed, OSCN-P. (D) Water escape structures in sandstone beds, closely adjacent to beds in Fig. 13D. (E) Stacked, tabular centimetre to decimetre-scale beds, fining-upward from very fine muddy sands in basal beds, to muds and clays in between, unit OSCN-P. (F) Tabular sand beds, OSCN-P, showing transition from planar to ripple laminae. (G) Irregular stacking pattern of sand beds in unit OSCN-P; rock hammer is 32 cm long.

Fig. 17: Sand-dominated lithofacies in thin section. (A) OSCN-P, showing lowermost bed in centimetre-scale fining-upward sequence. Sand content decreases in overlying beds. (B) Textural histogram of 139 individually measured detrital grains, same sample as above. (C) Pie chart showing overall sediment composition. (D) Massive sand bed at top of measured section, OSCS-H, showing well-cemented quartzite. (E) Textural classification for sample shown in (D). (F) Pie chart showing composition of sample taken from OSCS-H.

Fig 18: A) Marinoan bathymetric curve for the Adelaide Rift Complex, from Preiss (2000). The red square highlights the approximate stratigraphic location of (B), sequence stratigraphic interpretation of the relationship between the Wonoka Formation, Billy Springs Formation and Wilpena Group. HST = Highstand Systems Tract, MFS = Maximum Flooding Surface. Influenced by Dyson (2003).

Fig. 19: (A) Diapirs of the northern Flinders Ranges. Modified from Coats (1973). (B) North to south cross-section through the Flinders Ranges, showing synforms and antiforms as the product of salt mobilization. Modified from Rowan & Vendeville (2006). Left hand portion of cross-section corresponds to line in (A). (C) Current Gulf of Mexico topography, showing surface expression of active salt-withdrawal minibasins. Modified from NOAA (2015) (http://www.ncddc.noaa.gov/website/google_maps/OE/mapsOE.htm).

REFERENCES

Ala, M.A. (1974) Salt diapirism in southern Iran. *AAPG Bull.*, 58, 1758-1770.

Arbués, P., Ferrrer, O., Roca, E., Giles, K., Rowan, M., De Matteis, M., and **Muñoz, J.A.** (2012) The Bakio salt wall and its effects on synkinematic deepwater sedimentation (Basque Pyrenees, Northern Spain). *EGU General Assembly Conference Abstracts* **14**, 9659.

Archer, A.W. (1991) Modeling of tidal rhythmites using modern tidal periodicities and implications for short-term sedimentation rates. In: *Sedimentary Modeling: Computer Simulations and Methods for Improved Parametre Definition (*Ed. E Franseen), *Bull. Kansas State Geol. Surv.* 233, 185-194.

Aschoff, J.L., and **Giles, K.A.** (2005) Salt diapir-influenced, shallow-marine sediment dispersal patterns: Insights from outcrop analogs. *AAPG Bull.*, **89**, 447-469.

Banham, S.G., and **Mountney, N.P.** (2013a) Evolution of fluvial systems in salt-walled mini-basins: A review and new insights. *Sed. Geol.*, **296**, 142-166.

Banham, S.G., and **Mountney, N.P.** (2013b) Controls on fluvial sedimentary architecture and sediment-fill state in salt-walled mini-basins: Triassic Moenkopi Formation, Salt Anticline Region, SE Utah, USA. *Basin Res.* **25**, 709-737.

Banham, S.G., and **Mountney, N.P.** (2014) Climatic versus halokinetic control on sedimentation in a dryland fluvial succession. *Sedimentology*, **61**, 570-608.

Bao, H., Chen, Z.Q., and **Zhou, C.** (2012) An ^{17}O record of late Neoproterozoic glaciation in the Kimberley region, Western Australia. *Precambrian Res.*, **216**, 152-161.

Barde, J.P., Chamberlain, P., Galavazi, M., Gralla, P., Harwijanto, J., Marsky, J., and **van den Belt, F.** (2002) Sedimentation during halokinesis: Permo-Triassic reservoirs of the Saigak field, Precaspian basin, Kazakhstan. *Petroleum Geoscience*, **8**, 177-187.

Beaubouef, R.T., and **Friedmann, S.J.** (2000) High resolution seismic/sequence stratigraphic framework for the evolution of Pleistocene intra slope basins, western Gulf of

Mexico: depositional models and reservoir analogs. In: *Deep-water reservoirs of the world.* (Ed. P. Weimer) *20th GCSSEPM Bob F. Perkins Research Conference*, 40-60.

Beaubouef, R.T., Abreu, V., and **Van Wagoner, J.C.** (2003). Basin 4 of the Brazos-Trinity slope system, western Gulf of Mexico: The terminal portion of a late Pleistocene lowstand systems tract. In: *Shelf margin deltas and linked down slope petroleum systems: Global significance and future exploration potential* (Eds. H.R. Roberts, N.C. Rosen, R.F. Fillon, and J.B. Anderson) *23rd GCSSEPM Bob F. Perkins Research Conference,* 45-66.

Bogdanova, S.V., Pisarevsky, S.A., and **Li, Z.X.** (2009) Assembly and breakup of Rodinia (some results of IGCP Project 440). *Stratigraphy and Geological Correlation*, **17**, 259-274.

Bouma, A.H., and **Bryant, W.R.** (1994) Physiographic features on the northern Gulf of Mexico continental slope. *Geo-Mar. Lett.,* **14**, 252-263.

Bowring, S., Myrow, P., Landing, E., Ramezani, J., and **Grotzinger, J.** (2003) Geochronological constraints on terminal Neoproterozoic events and the rise of metazoans. *Geophysical Research Abstracts*, **5**, 13219.

Brown Jr., L.F., Loucks, R.G., Trevio, R.H., and **Hammes, U.** (2004) Understanding growth-faulted, intraslope subbasins by applying sequence-stratigraphic principles: Examples from the south Texas Oligocene Frio Formation. *AAPG Bull.*, **88**, 1501-1522.

Bryant, W.R., Bryant, J.R., Feeley, M.H., and **Simmons, G.R.** (1990) Physiographic and bathymetric characteristics of the continental slope, northwest Gulf of Mexico. *Geo-Mar. Lett.* **10**, 182-199.

Callot, J.P., Ribes, C., Kergaravat, C., Bonnel, C., Temiz, H., Poisson, A., Vrielynck, B., Salel, J.F., and **Ringenbach, J.C.** (2014) Salt tectonics in the Sivas basin (Turkey): crossing salt walls and minibasins. *Bull. Soc. Géol. Fr.*, **185**, 33-42.

Campana, B., Coats, R.P., Horwitz, R.C., and **Webb, B.P.** (1961) UMBERATANA map sheet, 1:63,360 Series. South Australia Geological Survey, Adelaide.

Carto, S.L., and **Eyles, N.** (2012) Sedimentology of the Neoproterozoic (c. 580Ma) Squantum 'Tillite', Boston Basin, USA: Mass flow deposition in a deep-water arc basin lacking direct glacial influence. *Sed. Geol.*, **269**, 1-14.

Chumakov, N.M. (2009) The Baykonurian glaciohorizon of the late Vendian. *Stratigraphy and Geological Correlation*, **17**, 373-381.

Coats, R.P. (1973) COPLEY map sheet, 1:250,000 Series. South Australia Geological Survey, Adelaide.

Coats, R.P., and **Blissett, A.H.** (1971) Regional and economic geology of the Mt. Painter Province. *Bull. Geol. Surv. S. Aust.*, **43**, 426 pp.

Coats, R.P., and **Preiss, W.V.** (1980) Stratigraphic and geochronological reinterpretation of Late Proterozoic glaciogenic sequences in the Kimberley region, Western Australia. *Precambrian Res.*, **13**, 181-208.

Collie, A.J., and **Giles, K.,** 2011, Comparison of Lower Cambrian carbonate facies and halokinetic sequences in minibasins developed on opposite sides of the Wirrealpa Diapir, Central Flinders Ranges, South Australia. *AAPG Search and Discovery Article* #50442.

Corkeron, M.L., and **George, A.D.** (2001) Glacial incursion on a Neoproterozoic carbonate platform in the Kimberley region, Australia. *Geol. Soc. Am. Bull.*, **113**, 1121-1132.

Cowan, E.A., Cai, J., Powell, R.D., Seramur, K.C., and **Spurgeon, V.L.** (1998) Modern tidal rhythmites deposited in a deep-water estuary. *Geo-Mar. Lett.*, **18**, 40-48.

Cowan, E.A., Seramur, K.C., Cai, J., and **Powell, R.D.** (1999) Cyclic sedimentation produced by fluctuations in meltwater discharge, tides and marine productivity in an Alaskan fjord. *Sedimentology*, **46**, 1109-1126.

Curtis J.W., Jenkins, G.W. and **Gravestock, D.I.** (1991) Mississippi valley type Lead-Zinc mineralization northern Flinders Ranges, South Australia. *Geological Survey of South Australia Report Book*, **91/102**, 280 pp.

Dalgarno, C.R., and **Johnson, J.E.** (1968) Diapiric structures and late Precambrian-early Cambrian sedimentation in Flinders Ranges, South Australia. In: *Diapirism and Diapirs.* (Eds. J. Braunstein and G.D. O'Brien) *AAPG Mem.* **8**, 301-314.**Davison, I., Bosence, D., Alsop, G.I.,** and **Al-Aawah, M.H.** (1996) Deformation and sedimentation around active Miocene salt diapirs on the Tihama Plain, northwest Yemen. *Geol. Soc. London Spec. Publ.*, **100**, 23-39.

DiBona, P. (1989) Geological history and sequence stratigraphy of the Late Proterowic Wonoka Formation, Northern Flinders Ranges, South Australia. Flinders University Ph.D. thesis (unpublished).

DiBona, P.A., Von der Borch, C.V.D., and **Christie-Blick, N.** (1990) Sequence stratigraphy and evolution of a basin-slope succession: The Late Proterozoic Wonoka Formation, Flinders Ranges, South Australia. *Aust. J. Earth Sci.*, **37**, 135-145.

DiBona, P.A. (1991) A previously unrecognised Late Proterozoic succession: Upper Wilpena Group, northern Flinders Ranges, South Australia. *Quarterly Geological Notes Geological Survey of South Australia*, **117**, 2-9.

Direen, N.G., and **Jago, J.B.** (2008) The Cottons Breccia (Ediacaran) and its tectonostratigraphic context within the Grassy Group, King Island, Australia: A rift-related gravity slump deposit. *Precambrian Res.*, **165**, 1-14.

Drexel, J.F., Preiss, W.V., and **Parker, A.J.,** (Eds) (1993) The Geology ofSouth Australia, vol. 1, Precambrian. *Bull. Geol. Surv. S. Aust.,* **54**, 242 pp..

Dyson, I.A. (1996) A new model for diapirism in the Adelaide Geosyncline. *MESA Journal*, **3**, 41-48.

Dyson, I.A. (1999) The Beltana Diapir–a salt withdrawal minibasin in the northern Flinders Ranges. *MESA Journal*, **15**, 40-46.

Dyson, I.A. (2001). The diapir-base metal association in the northern Flinders Ranges. *MESA Journal*, **22**, 37-43.

Dyson, I.A. (2004) Interpreted shallow and deep water depositional systems of the Beltana mini-basin in the northern Flinders Ranges, South Australia. In: *Salt-sediment interactions and hydrocarbon prospectivity: Concepts, Applications, and Case Studies for the 21st Century* (Eds P.J. Post, D.L. Olson, K.T. Lyons, S.L. Palmes, P.F. Harrison and N.C. Rosen) *GCSSEPM Bob F. Perkins Research Conference*, 997-1030.

Dyson, I.A.(2004a) Christmas Tree Diapirs and Development of Hydrocarbon Reservoirs: A Model from the Adelaide Geosyncline, South Australia. In: *Salt-sediment interactions and hydrocarbon prospectivity: Concepts, Applications, and Case Studies for the 21st Century* (Eds P.J. Post, D.L. Olson, K.T. Lyons, S.L. Palmes, P.F. Harrison and N.C. Rosen) *24th GCSSEPM Bob F. Perkins Research Conference*, 133-165.

Dyson, I.A. (2005) Formation of submarine unconformities in halotectonic mini-basins during passive margin development of the Adelaide Geosyncline, South Australia. In: *Petroleum Systems of Divergent Continental Margin Basins*. (Eds P.J. Post, N.C. Rosen, D.L. Olson, S.L. Palmes, K.T. Lyons, and G.B. Newton) *25th GCSSEPM Bob F. Perkins Research Conference*, 679-721.

Dyson, I.A., and **Marshall, T.R.** (2007) Neoproterozoic salt nappe complexes and salt-withdrawal mini-basins in the Amadeus Basin. In: *Proceedings of the Central Australian Basins Symposium (CABS), Alice Springs, Northern Territory, 16–18 August, 2005* (Eds. T.J. Munson and G.J. Ambrose), 16-18.

Dyson I.A., and **Rowan, M.G.** (2004) Geology of a Welded Diapir and Flanking Mini-Basins in the Flinders Ranges of South Australia In: *Salt-sediment interactions and hydrocarbon prospectivity: Concepts, Applications, and Case Studies for the 21st Century*

(Eds P.J. Post, D.L. Olson, K.T. Lyons, S.L. Palmes, P.F. Harrison and N.C. Rosen) *GCSSEPM Bob F. Perkins Research Conference*, 69-89.

Eyles, N., and **Januszczak, N.** (2004) 'Zipper-rift': a tectonic model for Neoproterozoic glaciations during the breakup of Rodinia after 750 Ma. *Earth-Sci. Rev.*, **65**, 1-73.

Ferrer, O., Arbues, P., Roca, E., Giles, K., Rowan, M.G., De Matteis, M., and **Munoz, J.A.,** (2014) Effect of Diapir Growth on Synkinematic Deepwater Sedimentation: the Bakio Diapir (Basque-Cantabrian Basin, Northern Spain). *AAPG Search and Discovery Article* #90189.

Flint, D.J., and **Webb, A.W.,** (1980) Geochronological investigations of the Willyama Complex, South Australia. *South Australia Department of Mines and Energy Report Book*, **79/163**.

Forbes, B.G. (1966) The geology of the Marree 1: 250,000 map area. *Department of Mines Report of Investigations,* **28**.

Forbes, B.G. (1971). Stratigraphic subdivision of the Pound Quartzite (late Precambrian, South Australia). *Trans. Roy. Soc. S. Aust.* **95**, 219-225.**Gehling, J.G.** (2000) Environmental interpretation and a sequence stratigraphic framework for the terminal Proterozoic Ediacara Member within the Rawnsley Quartzite, South Australia. *Precambrian Res.,* **100**, 65-95.

Gehling, J.G., (1982) Sedimentology and Stratigraphy of the Late Precambrian Pound Subgroup, Central Flinders Ranges, S.A. *University of Adelaide MSc thesis.*

Giles, K.A., and **Lawton, T.F.** (2002) Halokinetic sequence stratigraphy adjacent to the El Papalote diapir, northeastern Mexico. *AAPG Bull.*, **86**, 823-840.

Grey, K., and **Corkeron, M.** (1998) Late Neoproterozoic stromatolites in glacigenic successions of the Kimberley region, Western Australia: evidence for a younger Marinoan glaciation. *Precambrian Res.*, **92**, 65-87.

Hearon, T.E., Rowan, M.G., Lawton, T.F., Hannah, P.T., and **Giles, K.A.** (2014) Geology and tectonics of Neoproterozoic salt diapirs and salt sheets in the eastern Willouran Ranges, South Australia. *Basin Res.*, (early view) doi: 10.1111/bre.12067.

Hearon, T.E., Rowan, M.G., Lawton, T.F., Hannah, P.T., and **Giles, K.A.** (2015) Geology and tectonics of Neoproterozoic salt diapirs and salt sheets in the eastern Willouran Ranges, South Australia. *Basin Res.* **27**, 183-207.

Hebert, C.L., Kaufman, A.J., Penniston-Dorland, S.C., and **Martin, A.J.** (2010) Radiometric and stratigraphic constraints on terminal Ediacaran (post-Gaskiers) glaciation and metazoan evolution. *Precambrian Res.*, **182**, 402-412.

Hebert, C.L., Kaufman, A.J., Penniston-Dorland, S.C., and **Martin, A.J.** (2010) Radiometric and stratigraphic constraints on terminal Ediacaran (post-Gaskiers) glaciation and metazoan evolution. *Precambrian Res.*, **182**, 402-412.

Hoffman, P.F., and **Li, Z.X.** (2009) A palaeogeographic context for Neoproterozoic glaciation. *Palaeogeogr. Palaeoclimatol. Palaeoecol.*, **277**, 158-172.

Hoffman, P.F., and **Schrag, D.P.** (2002) The snowball Earth hypothesis: testing the limits of global change. *Terra Nova*, **14**, 129-155.

Hoffman, P.F., Calver, C.R., and **Halverson, G. P.** (2009) Cottons Breccia of King Island, Tasmania: Glacial or non-glacial, Cryogenian or Ediacaran? *Precambrian Res.*, **172**, 311-322. Jackson, 2012

Jackson, M.P.A., and **Harrison, J.C.** (2006) An allochthonous salt canopy on Axel Heiberg Island, Sverdrup Basin, Arctic Canada. *Geology*, **34**, 1045-1048.

Jenkins, R., Haines, P.W., and **Gostin, V.A.** (1988) The Ediacaran revisited. *Geological Society of Australia Abstracts*, **21**, 203-204

Jenkins, R.J. (2011) Billy Springs Glaciation, South Australia. In *The Geological Record of Neoproterozoic Glaciations* (Eds E. Arnaud, G.P. Halverson, and G. Sheilds-Zhou) *Geol. Soc. London Mem.*, **36**, 693-699.

Johnson, S.P. (2013) The Birth of Supercontinents and the Proterozoic Assembly of Western Australia. Geological Survey of Western Australia, 78 pp.

Kernen, R.A., Giles, K.A., Rowan, M.G., Lawton, T.F., and **Hearon, T.E.** (2012) Depositional and halokinetic-sequence stratigraphy of the Neoproterozoic Wonoka Formation adjacent to Patawarta allochthonous salt sheet, Central Flinders Ranges, South Australia. *Geol. Soc. Lond. Spec. Publ.* **363**, 81-105.

Kvale, E.P., Cutright, J., BIlodeau, D., Archer, A., Johnson, H.R., and **Pickett, B.** (1995) Analysis of modern tides and implications for ancient tidalites. *Cont. Shelf Res.*, **15**, 1921-1943.

Lamb, M.P., Toniolo, H., and **Parker, G.** (2006) Trapping of sustained turbidity currents by intraslope minibasins. *Sedimentology*, **53**, 147-160.

Laudon, R.C. (1984) Evaporite diapirs in the La Popa basin, Nuevo Leon, Mexico. *Geol. Soc. Am. Bull.*, **95**, 1219-1225.

Lemon, N.M. (1985). Physical modeling of sedimentation adjacent to diapirs and comparison with late Precambrian Oratunga breccia body in central Flinders Ranges, South Australia. *AAPG Bull.*, **69**, 1327-1338.

Lemon, N.M. (2000) A Neoproterozoic fringing stromatolite reef complex, Flinders Ranges, South Australia. *Precambrian Res.*, **100**, 109-120.

Li, Z.X., Bogdanova, S.V., Collins, A.S., Davidson, A., De Waele, B., Ernst, R.E., Fitzsimons, I.C.W., Fuck, R.A., Gladkochub, D.P., Jacobs, J., Karlstrom, K.E., Lu, S., Natapov, L.M., Pease, V., Pisarevsky, S.A., Thrane, K., and **Vernikovsky, V.** (2008)

Assembly, configuration, and break-up history of Rodinia: a synthesis. *Precambrian Res.,* **160**, 179-210.

Li, Z.X., Evans, D.A., and **Halverson, G.P.** (2013) Neoproterozoic glaciations in a revised global palaeogeography from the breakup of Rodinia to the assembly of Gondwanaland. *Sed. Geol.*, **294**, 219-232.

Madof, A.S., Christie-Blick, N., and **Anders, M.H.** (2009) Stratigraphic controls on a salt-withdrawal intraslope minibasin, north-central Green Canyon, Gulf of Mexico: Implications for misinterpreting sea level change. *AAPG Bull.*, **93**, 535-561.

Mallarino, G., Beaubouef, R.T., Droxler, A.W., Abreu, V., and **Labeyrie, L.** (2006) Sea level influence on the nature and timing of a minibasin sedimentary fill (northwestern slope of the Gulf of Mexico). *AAPG Bull.*, **90**, 1089-1119.

Mannie, A.S., Jackson, C.A.L., and **Hampson, G.J.** (2014) Shallow-marine reservoir development in extensional diapir-collapse minibasins: An integrated subsurface case study from the Upper Jurassic of the Cod terrace, Norwegian North Sea. *AAPG Bull.*, **98**, 2019-2055.

Matthews, W.J., Hampson, G.J., Trudgill, B.D., and **Underhill, J.R.** (2007) Controls on fluviolacustrine reservoir distribution and architecture in passive salt-diapir provinces: Insights from outcrop analogs. *AAPG Bull.*, **91**, 1367-1403.

Mazumder, R., and **Arima, M.** (2013) Tidal rhythmites in a deep sea environment: An example from Mio-Pliocene Misaki Formation, Miura Peninsula, Japan. *Mar. Petrol. Geol.*, **43**, 320-325.

Narbonne, G.M. (2005) The Ediacara biota: Neoproterozoic origin of animals and their ecosystems. *Annu. Rev. Earth Planet. Sci.*, **33**, 421-442.

Newell, A.J., Benton, M.J., Kearsey, T., Taylor, G., Twitchett, R.J., and **Tverdokhlebov, V.P.** (2012) Calcretes, fluviolacustrine sediments and subsidence patterns in Permo-Triassic salt-walled minibasins of the south Urals, Russia. *Sedimentology*, **59**, 1659-1676.

Olson, H.C., & **Damuth, J.E.** (2010) Character, Distribution and Timing of Latest Quaternary Mass-Transport Deposits in Texas—Louisiana Intraslope Basins Based on High-Resolution (3.5 kHz) Seismic Facies and Piston Cores. In: *Submarine Mass Movements and Their Consequences* (Eds. D.C. Mosher, L. Moscardelli, R.C. Shipp, J.D. Chaytor, C.D.P. Baxter, H.J. Lee, and R. Urgeles) pp. 607-617. Springer, Netherlands.

Paul, E., **Flöttmann, T.**, and **Sandiford, M.** (1999) Structural geometry and controls on basement-involved deformation in the northern Flinders Ranges, Adelaide Fold Belt, South Australia. *Aust. J. Earth Sci.*, **46**, 343-354.

Pell, S.D., McKirdy, D.M., Jansyn, J., and **Jenkins, R.J.F.** (1993) Ediacaran carbon isotope stratigraphy of South Australia—An initial study. *Trans. Roy. Soc. S. Aust.*, **117**, 153-161.

Pickering, K.T., Hiscott, R.N., and **Hein, F.J.** (1989) Contourite drifts. In: *Deep-Marine Environments: Clastic Sedimentation and Tectonics.* pp. 219-245. Unwin Hyman, London.

Pilcher, R.S., Kilsdonk, B., and **Trude, J.** (2011) Primary basins and their boundaries in the deep-water northern Gulf of Mexico: Origin, trap types, and petroleum system implications. *AAPG Bull.*, **95**, 219-240.

Plummer, P.S. (1978) Note on the palaeoenvironmental significance of the Nuccaleena Formation (upper Precambrian), central Flinders Ranges, South Australia. *J. Geol. Soc. Aust.*, **25**, 395-402.

Poprawski, Y., **Basile, C.**, **Agirrezabala, L.M.**, **Jaillard, E.**, **Gaudin, M.**, and **Jacquin, T.** (2014) Sedimentary and structural record of the Albian growth of the Bakio salt diapir (the Basque Country, northern Spain). *Basin Res.*, **26**, 746-766.

Posamentier, H.W., and **Allen, G.P.** (1999) Siliciclastic sequence stratigraphy: concepts and applications (Vol. 7). SEPM (Society for Sedimentary Geology), Tulsa, 204 pp.

Postma, G., Nemec, W., and **Kleinspehn, K.L.** (1988). Large floating clasts in turbidites: a mechanism for their emplacement. *Sed. Geol.*, **58**, 47-61.

Prather, B.E. (2000) Calibration and visualization of depositional process models for above-grade slopes: a case study from the Gulf of Mexico. *Mar. Petrol. Geol.*, **17**, 619-638.

Preiss, W.V. (Compiler), 1987, The Adelaide Geosyncline—late Proterozoic stratigraphy, sedimentation, paleontology and tectonics. *Bull. Geol. Surv. S. Aust.,* **53**, 438 pp..

Preiss, W.V. (1990) A stratigraphic and tectonic overview of the Adelaide Geosyncline, South Australia. In: *The Evolution of a Late Precambrian–Early Palaeozoic Rift Complex: The Adelaide Geosyncline*, (Eds J.B. Jago and P.S. Moore) *Geol. Soc. Aust. Spec. Publ.*, 16, 1-33.

Preiss, W.V. (1999) Parachilna, South Australia, sheet SH54-13 2nd edn. 1: 250 000 geological series explanatory notes. PIRSA, Adelaide, 52 pp.

Preiss, W.V. (2000), The Adelaide Geosyncline of South Australia and it's significance in Neoproterozoic continental reconstruction. *Precambrian Res.* **100**, 21-63.

Rebesco, M., Hernández-Molina, F.J., Van Rooij, D., and **Wåhlin, A.** (2014) Contourites and associated sediments controlled by deep-water circulation processes: State-of-the-art and future considerations. *Mar. Geol.*, **352**, 111-154.

Reid, P.W. (1992) Stratigraphy, Structure, and Stable Isotope Analysis of the Billy Springs Formation, Mt. Freeling Syncline, S.A. *University of Adelaide Honors Thesis*, unpublished.

Reilly, M. (2001) Deepwater Reservoir Analogue – Bunkers Sandstone, Donkey Bore Syncline, Flinders Ranges Australia. *University of Adelaide Honours Thesis*, unpublished.

Ribes, C., Kergaravat, C., Bonnel, C., Crumeyrolle, P., Callot, J.P., Poisson, A., Temiz, H., and **Ringenbach, J.C.** (2015) Fluvial sedimentation in a salt-controlled mini-basin: stratal patterns and facies assemblages, Sivas Basin, Turkey. *Sedimentology*, 62, 1513-1545.

Ringenbach, J.C., Salel, J.F., Kergaravat, C., Ribes, C., Bonnel, C., and **Callot, J.P.** (2013) Salt tectonics in the Sivas Basin, Turkey: outstanding seismic analogues from outcrops. *First Break*, **31**, 93-101.

Rowan, M.G., and **Vendeville, B.C.** (2006) Foldbelts with early salt withdrawal and diapirism: physical model and examples from the northern Gulf of Mexico and the Flinders Ranges, Australia. *Mar. Petrol. Geol.*, **23**, 871-891.

Rowan, M.G., Lawton, T.F., Giles, K.A., and **Ratliff, R.A.** (2003) Near-salt deformation in La Popa basin, Mexico, and the northern Gulf of Mexico: A general model for passive diapirism. *AAPG Bull.*, **87**, 733-756.

Saura, E., Vergés, J., Martín-Martín, J.D., Messager, G., Moragas, M., Razin, P., Grélaud, C., Joussiaume, R., Malaval, M., Homke, S., and **Hunt, D.W.** (2014) Syn-to post-rift diapirism and minibasins of the Central High Atlas (Morocco): the changing face of a mountain belt. *J. Geol. Soc. London,* **171**, 97-105.

Shanmugam, G. (1980) Rhythms in deep sea, fine-grained turbidite and debris-flow sequences, Middle Ordovician, eastern Tennessee. *Sedimentology*, **27**, 419-432.

Shanmugam, G. (2008) Deep-water bottom currents and their deposits. In: *Contourites* (Eds M. Rebesco and A. Camerlenghi), *Dev. Sedimentol,*.**60**, 59-81.

Sheard, M.J. (2012) Explanatory Notes for MARREE 1:250 000 Geological Map, sheet SH 54-5. Report Book 2012/00004. Department for Manufacturing, Innovation, Trade, Resources and Energy, South Australia, Adelaide, 231 pp.

Shultz, M.R., and **Hubbard, S.M.** (2005) Sedimentology, stratigraphic architecture, and ichnology of gravity-flow deposits partially ponded in a growth-fault-controlled slope minibasin, Tres Pasos Formation (Cretaceous), southern Chile. *J. Sed. Res.*, **75**, 440-453.

Stow, D.A., and **Mayall, M.** (2000) Deep-water sedimentary systems: new models for the 21st century. *Mar. Petrol. Geol.*, 17, 125-135.

Stow, D.A.V., and **Piper, D.J.W**. (1984) Deep-water fine-grained sediments: facies models. *Geol. Soc. London Spec. Publ.*, 15, 611-646.

Stow, D.A.V., Reading, H.G., and **Collinson, J.D.** (1996) Deep seas. In: *Sedimentary environments: processes, facies and stratigraphy* (Ed. H.G. Reading) 3rd edn, pp. 395-453, Blackwell Science, Oxford.

Stow, D.A.V., Huc, A.Y., and **Bertrand, P.** (2001). Depositional processes of black shales in deep water. *Mar. Petrol. Geol.*, **18**, 491-498.

Strachan, L.J. (2008) Flow transformations in slumps: a case study from the Waitemata Basin, New Zealand. *Sedimentology*, **55**, 1311-1332.

Trudgill, B.D. (2011). Evolution of salt structures in the northern Paradox Basin: controls on evaporite deposition, salt wall growth and supra-salt stratigraphic architecture. *Basin Res.,* **23**, 208-238.

Trudgill, B.D., and **Paz, M.** (2009) Restoration of mountain front and salt structures in the northern Paradox Basin, SE Utah, In: *The Paradox Basin Revisited – New Developments in Petroleum Systems and Basin Analysis*. (eds. Houston, W.S., Wray, L.L., and Moreland, P.G.) RMAG Special Publication, pp. 132-177.

Trudgill, B., Banbury, N., and **Underhill, J.** (2004) Salt evolution as a control on structural and stratigraphic systems: northern Paradox foreland basin, southeast Utah, USA. In: *Salt–Sediment Interactions and Hydrocarbon Prospectivity: Concepts, Applications, and Case*

Studies for the 21st century.(Eds. P. Post, D. Olson, K. Lyons, S. Palmes, P. Harrison, and N. Rosen) *24th Annual GCSSEPM Bob F. Perkins Research Conference*, 669-700.

Venus, J.H., **Mountney, N.P.**, and **McCaffrey, W.D.** (2015) Syn-sedimentary salt diapirism as a control on fluvial-system evolution: an example from the proximal Permian Cutler Group, SE Utah, USA. *Basin Res.*, **27**, 152-182.

Von der Borch, C.C., and **Grady, A.E.** (1982) Wonoka Formation and Billy Springs Beds: Reconnaissance Interpretation. *Trans. Roy. Soc. S. Aust.,* **106**, 217-219.

Von der Borch, C.C., Smit, R., and **Grady, A.E.** (1982) Late Proterozoic submarine canyons of Adelaide Geosyncline, South Australia. *AAPG Bulletin*, **66**, 332-347.

Weeks, W. (2010) *On Sea Ice*. University of Alaska Press, Fairbanks, 664 pp.

Williams, G.E. (1988) Cyclicity in the late Precambrian Elatina Formation, South Australia: solar or tidal signature? *Climatic Change*, 13,117-128.

Williams, G.E. (1990) Precambrian Cyclic Rhythmites: Solar-Climatic or Tidal Signatures? *Phil. Trans. Roy. Soc. London. Series A, Mathematical and Physical Sciences,* **330**, 445-458.

Winker, C.D. (1996) High-resolution seismic stratigraphy of a late Pleistocene submarine fan ponded by salt-withdrawal mini-basins on the Gulf of Mexico continental slope. Offshore Technology Conference Paper 8024, 619-628.

Location	Age/Formation	Environment of Deposition	Brief Description of Minibasin Sediments	Reference
Precaspian Basin, Kazakhstan	Permian–Triassic reservoirs, with topographic influence at present	Fluvio–lacustrine, terrestrial	Modern minibasin sedimentology used as an analogue for underlying minibasin reservoirs. Facies include braided fluvial channels and associated floodplain/overbank deposits; palaeosols, lacustrine sediments, evaporates from reprecipitated salt originating from salt walls	Barde et al. 2002
Ural Mountains, Russia	Permian–Triassic	Fluvio–lacustrine, terrestrial	Analogous to sediments described by Barde et al. in Kazakhstan; channel fill, lacustrine delta/sheet flood deposits, calcretes	Newell et al. 2012
Sivas Basin, Turkey	Oligocene–Miocene	Fluvial, braided stream, playa-lake, lacustrine,sSabkha, shallow marine	Clastics and carbonates formed in a generally continental setting in multiple minibasins, which are surrounded by salt walls. Sediments show lateral thickness variability, unconformities and grain-size changes	Ribes et al., 2015; Callot et al 2014; Ringenbach et al 2013
Paradox Basin, Utah, USA	Pennsylvanian–Triassic; Honaker Trail, Cutler, and Chinle formations	Fluvial–lacustrine; terrestrial	Channel sandstones, mudstones and and conglomerates, lacustrine muds, palaeosols, and aeolian deposits (in Chinle Formation), with numerous sedimentological features varying due to salt-related topographic changes	Matthews et al. 2007; Banham & Mountney 2013a
Paradox Basin, Utah, USA	Permian Cutler Group	Fluvial, aeolian	Detailed sedimentological study on the interaction between fluvial and aeolian sediments and salt movement; demonstrates clear influence of salt movement on fluvial architecture and the preservation of aeolian sediments	Venus et al., 2015;
Paradox Basin, Utah, USA	Pennsylvanian–Permian Paradox Formation and Cutler Group	Shallow marine, fluvial and alluvial	Restricted shallow marine sediments are the source of evaporites; alluvial and shallow marine clastics in the Cutler Group characterized by progradational sequences, and related successive minibasin development; limited sedimentological descriptions	Trudgill & Paz, 2009; Trudgill, 2011; Trudgill et al., 2004
Paradox Basin, Utah, USA	Triassic Moenkopi Formation	Dominantly fluvial/ alluvial plain	Sheet-like and braided fluvial and floodplain deposits in multiple minibasins, with stratigraphic architecture controlled by fluvial systems which are, in turn, controlled by accommodation space, sedimentation rate, salt wall topography, climate and other factors	Banham & Mountney 2013b, 2014

Sverdrup Basin, Nunavut, Canada	Multiple Palaeozoic–Cenozoic Formations	Various, including fluvial–deltaic	Limited sedimentology reported, although basin fill ranges from Carboniferous–Eocene and probably represents a wide range of envornments. In the lower Cretaceous. Isachsen Formation, channel sands and basal debris flows of mixed lithology clasts onlap allochthonous diapirs	Jackson & Harrison 2006
Northwest Yemen	Miocene	Alluvial–lacustrine–beach–shallow marine–reef; in an arid climate	Not described as a 'minibasin', but actively rising diapir influencing sedimentation processes and unit thicknesses. Debris flows, conglomerates, flanking reefs, growth faults and unconformities are common	Davison et al 1996
Flinders Ranges, South Australia	Cryogenian; Enorama Shale	Shallow marine–reefs and carbonate mounds	Exposed diapiric island colonized by stromatolites and calcimicrobes, later drownd by sea-level rise and deposition of the deepwater Enorama Shale	Lemon 2000
Finders Ranges, South Australia	Lower Cambrian; Hawker Group Carbonates	Platform carbonates–shoreface–reef–midslope	A range of lithologies including carbonate turbidites, debris flows, bioherms, sabkha and tidal flats. Clastics include shoreface sands. Sediments show significant lateral facies change adjacent to diapir	Collie & Giles 2011
Flinders Ranges, South Australia	Cryogenian–Ediacaran; Burra and Umberatana, Groups	Storm-influenced shallow marine and shoreface, subaerially exposed dolomitic flat	Dominantly siliciclastics comprising large-scale T–R sequences; some carbonates; olistostromes and other units thinning/fining away from margin of Oladdie diapir	Dyson & Rowan 2004
Flinders Ranges, South Australia	Ediacaran (Marinoan); Oratunga Diapir, Umberatana Group	Generally shallow marine	Limestones, dolomites, shales and sandstones that thin against the diapir margin; some fluvio-glacial sands/diamictites; several unconformities	Lemon 1985
Amadeus Basin , Northern Territory, Australia	Neoproterozoic–Early Cambrian	Generally shallow marine	Various siltstones, sandstones and carbonates within several individual minibasins; limited description of influence of halokinesis on sedimentology	Dyson & Marshall 2007
La Popa Basin, Mexico	Upper Cretaceous/lower Palaeogene; Delgado Sandstone Member	Shelf–shoreface–foreshore	Delgado Sandstone consists of a series of 5 to 20 m thick coarsening-upward parasequences, generally with shelf mudstones at the bases and shoreface sands at the tops. Several other units, including carbonates and mudstones, are present in the minibasin and remain undescribed	Aschoff & Giles 2005; also see Rowan et al 2003; Laudon 1984

Persian Gulf, Iran	Cretaceous–Tertiary	Shallow marine	Rudist shoals on diapir flanks, diapiric material in surrounding sediment; diapirs were likely emergent; substantial subsidence related to underlying withdrawal not described	Ala, 1974
Willouran Ranges, South Australia	Cryogenian–Ediacaran; Primarily Burra Group	Shallow water, peritidal shelf, with rare deeper, continental and glacial episodes	Sandstones, siltstones and carbonates. Diapir-derived conglomerate beds and laterally variable, rotated beds adjacent to diapir	Hearon et al 2014
Flinders Ranges, South Australia	Ediacaran; Sandison Subgroup	Shelf to shallow marine	Sandstones and shales–tempestites lower in section, coarsening upward to tidally influenced quartzites. Unit thickness changes and conglomerates on Beltana diapir flanks	Dyson 1999, 2004
Atlas Mountains, Morocco	Jurassic; multiple formations	Slope–shelf–mixed platform	Platform carbonates interfingering with hemipelagic and slope sediments, eventually shallowing upward to shallow marine and continental sediments; asymmetrical minibasins flanking salt weld hundreds to thousands of metres in thickness; limited description of sedimentology	Saura et al 2014
Pyrenees Mountains, Spain	Cretaceous (Albian), Bakio Diapir and surrounding formations	Shelf–slope–deepwater	Shelf/slope marls, limestones, carbonate debrites at base, diapir-derived breccias, and an upper siliciclastic unit containing turbidites separated by numerous unconformities	Ferrer et al., 2014 Arbues et al 2012; Poprawski et al., 2014
Flinders Ranges, South Australia	Cambrian; Hawker Group, Donkey Bore Syncline	Deepwater and slope	Carbonates, shales and sands deposited in several cycles. Abundant turbidites and gravity flow deposits within shales	Reilly, 2001
Flinders Ranges, South Australia	Ediacaran; Billy Springs Formation	Slope–deepwater	Thick mudstone succession with abundant intrabasinal slumps and rare diamictites, with sandy turbidites more common up section	Counts & Amos 2014 (this study)
Magellanes Foreland Basin, southern Chile, South America	Late Cretaceous; Cerro Toro and Tres Pasos formations	Continental slope	Stacked, bioturbated, tabular turbidite sands within silty mudstones, deposited in an intraslope minibasin. Growth faults, mud-rich chaotic deposits, coarsening-upward packages are common	Shultz & Hubbard 2005

Previous Investigations of the Billy Springs Formation

Author	Year	Type of Study	Notes	Correlation
Campana et al.	1961	1 : 63,360 map sheet	First detailed geological map of the area	Not specified
Forbes	1966	Mines Department Report	Initial, brief description of 5200 m thick Wilpena Group sediments near Mount Freeling; siltstones, sandstones, marbles, dolomite	Brachina and Wonoka formations
Coats & Blissett	1971	SA Geologic Survey Bulletin	Divided Mount Freeling sediments into upper shaly member and lower silty member; termed sediments 'Billy Springs Beds'. Noted slump structures and lenticular boulder breccia	"Below the Pound Quartzite"
Von der Borch & Grady	1982	Peer-reviewed publication	Reconnaissance study; measured a similar section to OSCS; noted slumps, a thick laminated unit; and a breccia with a variety of exotic lithologies, attributed to mass movement	Bonney Sandstone
Jenkins et al.	1988	Abstract	First interpretation of breccia/boulder beds as glacial in origin	Upper Wonoka/Lower Pound
Dibona	1989	PhD Thesis	Measured section in Umberatana Syncline, noted 1200 m of silts and sands, one diamictite bed	Uncertain
Dibona	1991	SA Geologic Survey Notes	Mapped Billy Springs in general near base of formation, noted synsedimentary slumped beds and diamictite; interpreted as glacial in origin	Uncertain
Reid	1992	Honours Thesis	Detailed mapping and measurement of sections in the Mount Freeling area, noted Ediacaran-type fossils and sandy sediments equivalent to Bonney Sandstone and Rawnsley Quartzite; shallowing-up succession	Pound Subgroup
Pell et al.	1993	Peer-reviewed	Isotope stratigraphy study, incorporating Billy Springs carbonates from Mount	Mid-Billy Springs to Upper Wonoka

		publication	Freeling	
Jenkins	2011	Peer-reviewed publication	Focuses on potential glacial origin of diamictite bed, emphasizing exotic nature of large clasts and deformed laminae, suggesting that they originate as dropstones	Wilpena Group/Pound Subgroup
Sheard	2012	Map sheet explanatory notes	Divided Billy Springs into four members in the Mount Freeling area; partially based on mapping of Reid (1992)	Lower two members correlate to Bonney Sandstone, upper members to Rawnsley Quartzite

Table 3: Brief Descriptions of Stratigraphic Units, Old Station Creek South (OSCS)

Wonoka Fm	Shale with sparse decimetre-scale tabular beds of very fine-grained sand and silt that increase in frequency upward
OSCS-A	At base, first appearance of slumping/folding/soft-sediment deformation. Matrix similar to shales below, but with coarser discontinuous beds of highly deformed muddy silts/sands (slump ‘pods’). Slumps have both sharp boundaries with exterior matrix, and also grade laterally into shalier sediments. Larger clasts throughout, but locally concentrated, especially in upper beds. Clasts range from granule to boulder size, and do not occur outside of slumped sediment. Clasts are composed of a wide range of lithologies, including chert, dolomite and limestone
OSCS-B	Very few slumps; planar-bedded grey-green silts/silty mudstone. Not fissile as in unit A
OSCS-C	Planar silts with discontinuous slump beds, similar to those seen below, but slumps are much rarer. Slump beds contain very few or no exotic clasts
OSCS-D	Slump beds of similar lithology to those below, but more continuous. Uppermost appearance of slumping in section. Few or no clasts present

OSCS-E	Thick, monotonous section of planar-laminated silty mudstone, laminated on a millimetre-scale. Laminae vary in clay/silt content, causing them to weather differentially. In places, laminae are rhythmic and somewhat regularly spaced. No larger clasts or significantly coarser material seen
OSCS-F	Top of unit not well-defined; base marked by first appearance of decimetre-scale tabular beds of very fine-grained sandstone with tepee/loading structures at bases and wavy and rippled tops. Sand beds rare upward through unit
OSCS-G	Monotonous planar-laminated silts, similar to OSCS-E, but with more restricted exposure
OSCS-H	Uppermost unit very fine to lower fine-grained, clean, white, quartz arenite. Faint cross-stratification present in tabular, planar beds. Exposed as rubbly

Table 4: Brief Descriptions of Stratigraphic Units, Old Station Creek North (OSCN)

Wonoka Fm	Greenish-grey fissile silty muds, interbedded with sparse lighter-coloured layers of carbonate-rich or coarser material
OSCN-A	Green and grey silty muds. All bedding in the form of slumping, complex folds and chaotic bedding. Slumps range from large, open, metre-scale folds to small, isoclinal complex structures. Laminae comprising folds are centimetre to millimetre-scale apart and weather differentially, indicating slight differences in composition. Large decimetre-scale clasts rare, compositionally similar to matrix
OSCN-B	Lithology indistinguishable from below, but without any slump structures. Planar-laminated at centimetre-scale (0.5 to 10.0 cm)
OSCN-C	Similar to Unit A, but with slump folds generally on a much smaller scale

OSCN-D	Interbedded silty muds (matrix) and thin silt laminae. Upper 1.7 m exposes asymmetrical ripples and centimetre-scale sandy lenses. Ten centimetre thick ‘slump’ bed near base of unit. Larger clasts rare
OSCN-E	Blocky base with slumped top
OSCN-F1	Similar lithology to lower Unit D. Grey silty matrix with very fine-grained sand interlaminae, some thicker beds with internal convolute laminae. Ball and pillow structures present in thicker, sandier layers. Base sharp but slightly undulating
OSCN-F2	Discontinuous slump unit – pinches out and grades laterally into planar beds
OSCN-F3	Planar-laminated/bedded unit similar to F1 below. Top contact deeply scoured by overlying Unit G. Bed thickness between laminae varies from millimetre to decimetre-scale. Minor slump beds present within unit
OSCN-G	Slumped beds, ranging from massive/structureless to chaotic, to large, open folds. Contains numerous large intraformational clasts of similar or identical lithology as surrounding matrix. Series of folds with near-vertical axes near the top
OSCN-H	Planar laminated with prominent centimetre-scale sandy interbeds. Centimetre-scale ripples in thicker beds. Sandier beds contain ball and pillow structures and contorted internal bedding
OSCN-I	Similar to Unit G – slumped and folded beds in a range of styles. More vertical beds near top weather ‘chalky’ and may have increased carbonate content. Numerous large, discrete clasts within folds, of similar or identical lithology except for colour
OSCN-J	Planar bedding, more fissile and disturbed-looking than other planar beds

OSCN-K	Chaotic/massive slump unit; no large-scale open folds or planar laminae visible. Larger clasts also present
OSCN-L	Planar-bedded grey/green siltstone/mudstone. Laminae more regularly spaced and rhythmic than below. Near top, gently undulating beds and laminae resemble HCS, with truncation surfaces cutting underlying beds. Possible cross-strata near top could be incipient slumps. Definite small-scale slump structures at top, grading into the larger-scale folds of unit M
OSCN-M	Very thick unit comprised of a range of slump morphologies and folds. Large clasts rare but present. Cleavage planes increasingly dominant, obscuring bedding. Unable to determine true vertical thickness – this unit is discontinuous, as evidenced by the presence of planar bedding in correlative outcrops exposed in downstream creek meander loops. See equivalent section adjacent
OSCN-N	Generally planar laminae, grading into 'shalier' type weathering/bedding near the top. Sandy lenses in the lower part. No large clasts seen in outcrop. Thicker, coarser, tabular beds visible near top, resembling turbidites. Near centre of unit, a channel-shaped bed containing slumped and folded strata cuts across planar beds/laminae. Truncation of planar laminae clearly visible
OSCN-N	Slumped and folded strata visible in main outcrop near base of unit. Thicker, coarser, tabular beds near top, resembling turbidites. Beds often have a clear fining-up structure at a decimetre-scale. Bedding is planar, tops of beds may be gently undulating but ripples are not usually present. Adjacent to the main outcrop of this unit, granule–cobble–boulder-sized clasts are abundant in the lower portion of the unit, where exposed. Laminae often warped/draped around clasts

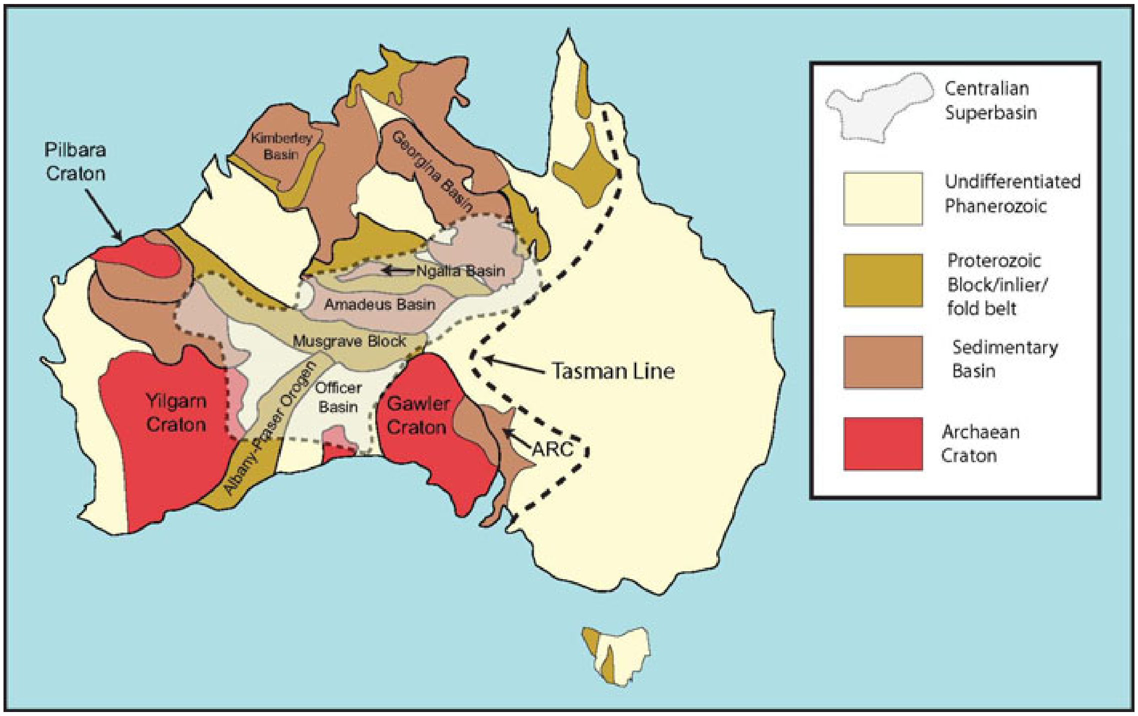
Pilbara Craton
Kimberley Basin
Georgina Basin
Ngalia Basin
Amadeus Basin
Musgrave Block
Tasman Line
Yilgarn Craton
Officer Basin
Albany-Fraser Orogen
Gawler Craton
ARC
Centralian Superbasin
Undifferentiated Phanerozoic
Proterozoic Block/inlier/ fold belt
Sedimentary Basin
Archaean Craton

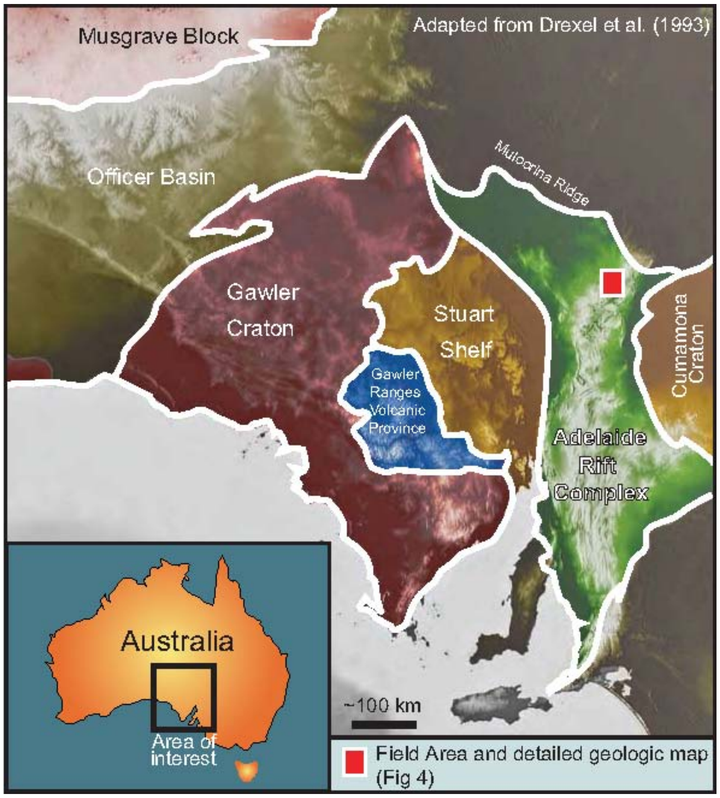
Musgrave Block
Adapted from Drexel et al. (1993)
Officer Basin
Mulooring Ridge
Gawler Craton
Stuart Shelf
Gawler Ranges Volcanic Province
Adelaide Rift Complex
Curnamona Craton
Australia
Area of interest
~100 km
Field Area and detailed geologic map (Fig 4)

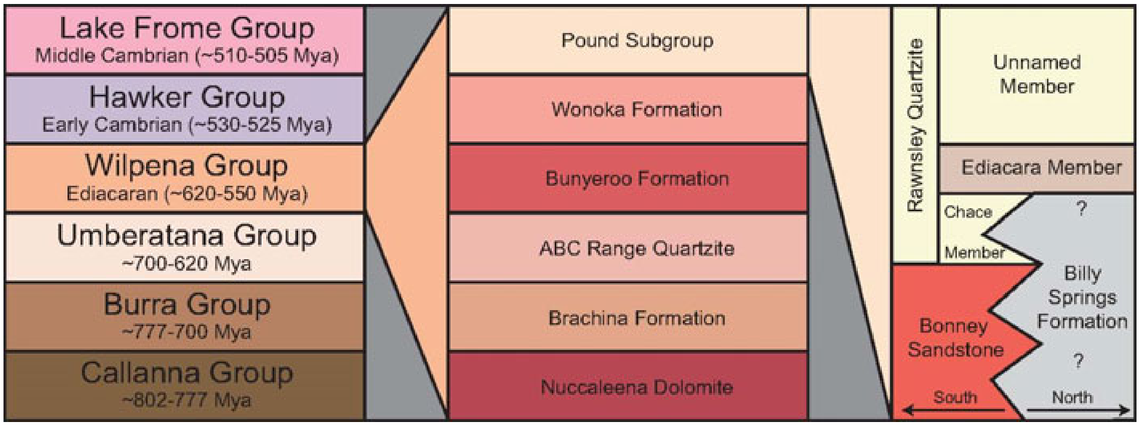

Lake Frome Group
Middle Cambrian (~510-505 Mya)
Hawker Group
Early Cambrian (~530-525 Mya)
Wilpena Group
Ediacaran (~620-550 Mya)
Umberatana Group
~700-620 Mya
Burra Group
~777-700 Mya
Callanna Group
~802-777 Mya
Pound Subgroup
Wonoka Formation
Bunyeroo Formation
ABC Range Quartzite
Brachina Formation
Nuccaleena Dolomite
Rawnsley Quartzite
Unnamed Member
Ediacara Member
Chace Member
?
Billy Springs Formation
?
Bonney Sandstone
South
North

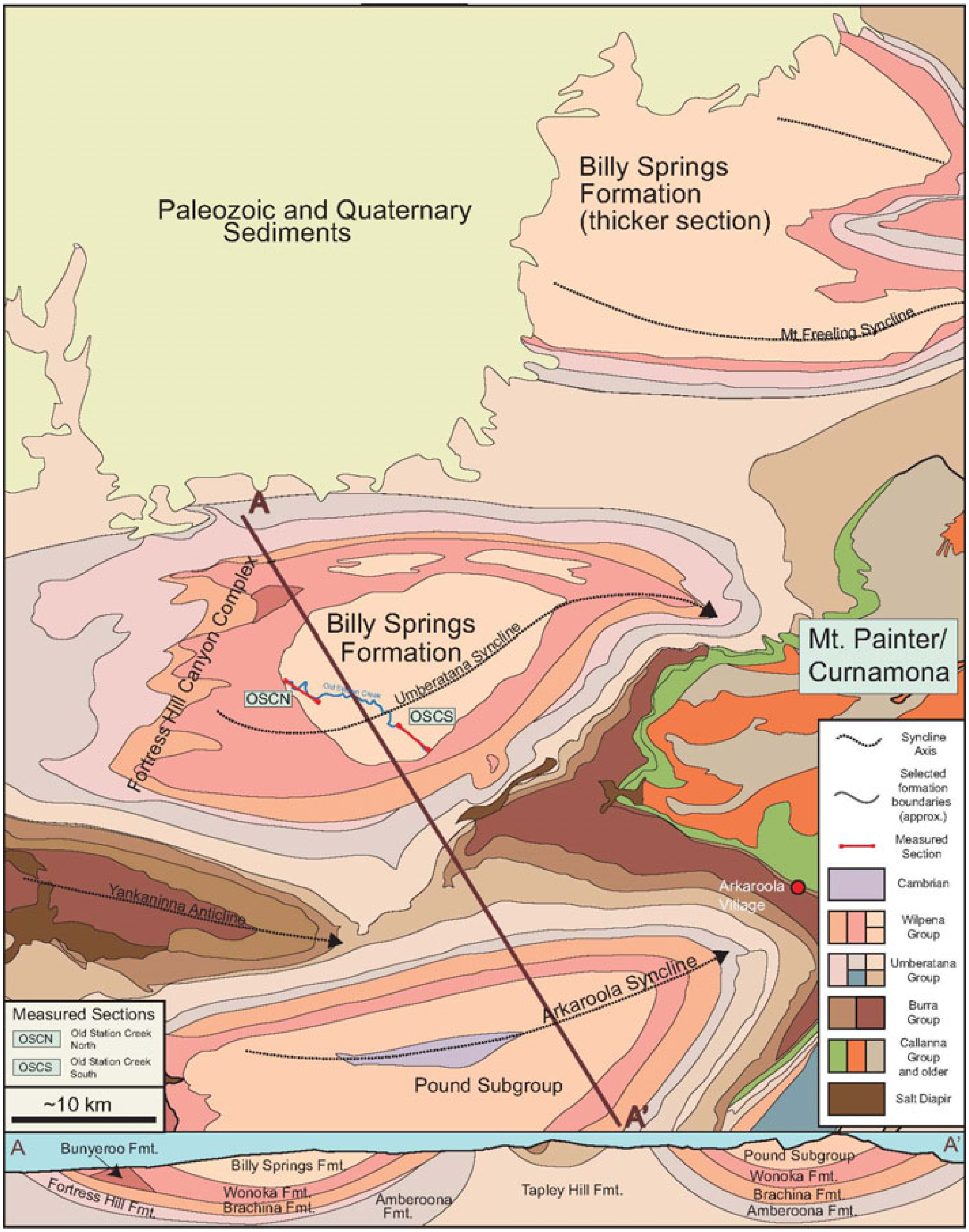

Paleozoic and Quaternary Sediments
Billy Springs Formation (thicker section)
Mt Freeling Syncline
A
Fortress Hill Canyon Complex
Billy Springs Formation
Umberatana Syncline
Old Station Creek
OSCN
OSCS
Mt. Painter/ Curnamona
Yankaninna Anticline
Arkaroola Village
Arkaroola Syncline
Pound Subgroup
A'
Measured Sections
OSCN Old Station Creek North
OSCS Old Station Creek South
~10 km
Syncline Axis
Selected formation boundaries (approx.)
Measured Section
Cambrian
Wilpena Group
Umberatana Group
Burra Group
Callanna Group and older
Salt Diapir
A
Bunyeroo Fmt.
Billy Springs Fmt.
Fortress Hill Fmt.
Wonoka Fmt.
Brachina Fmt.
Amberoona Fmt.
Tapley Hill Fmt.
Pound Subgroup
Wonoka Fmt.
Brachina Fmt.
Amberoona Fmt.
A'

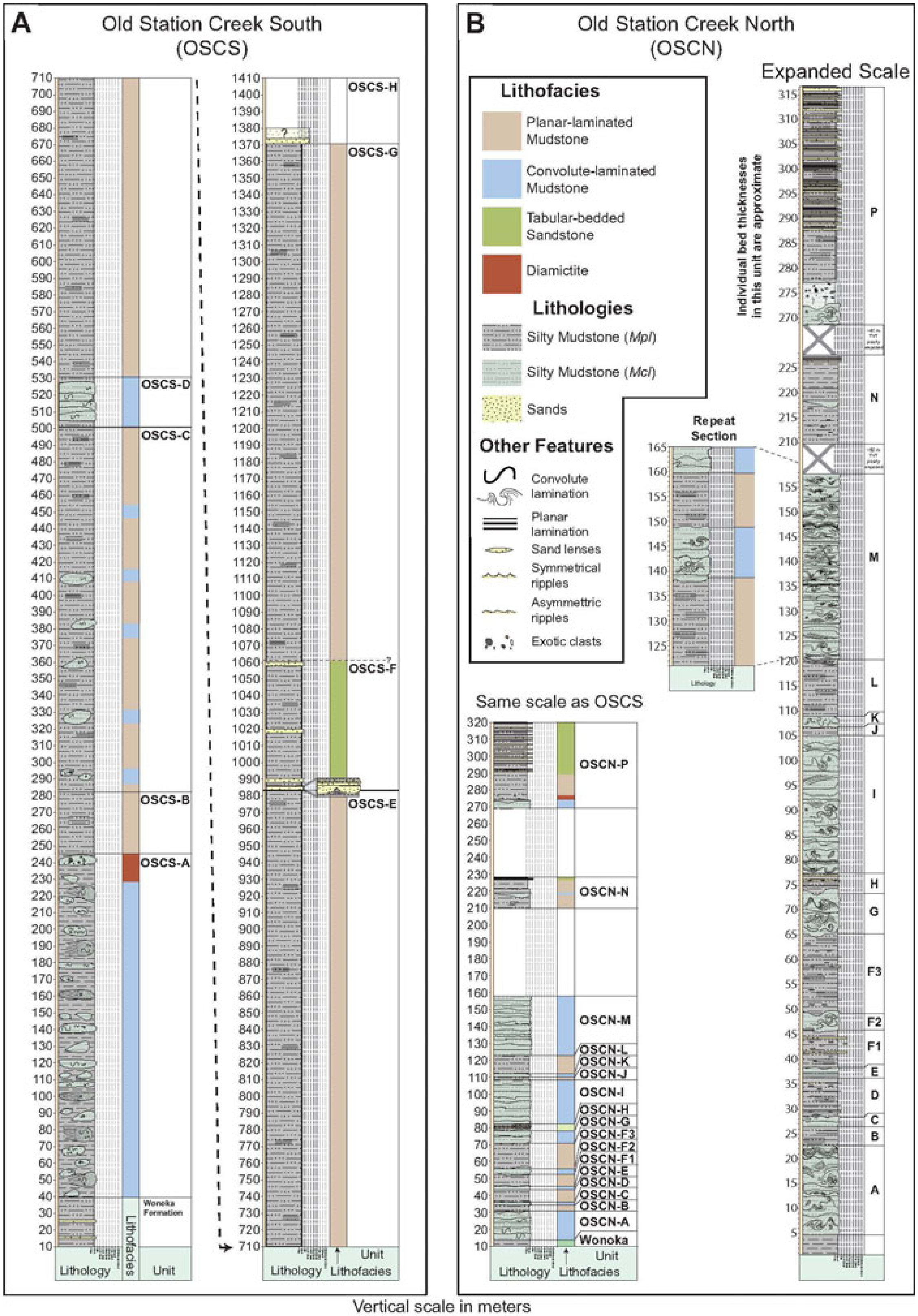
A
Old Station Creek South (OSCS)
OSCS-H
OSCS-G
OSCS-F
OSCS-E
OSCS-D
OSCS-C
OSCS-B
OSCS-A
Wonoka Formation
Lithology
Lithofacies
Unit
B
Old Station Creek North (OSCN)
Lithofacies
Planar-laminated Mudstone
Convolute-laminated Mudstone
Tabular-bedded Sandstone
Diamictite
Lithologies
Silty Mudstone (Mpl)
Silty Mudstone (Mcl)
Sands
Other Features
Convolute lamination
Planar lamination
Sand lenses
Symmetrical ripples
Asymmettric ripples
Exotic clasts
Repeat Section
Expanded Scale
Individual bed thicknesses in this unit are approximate
Same scale as OSCS
OSCN-P
OSCN-N
OSCN-M
OSCN-L
OSCN-K
OSCN-J
OSCN-I
OSCN-H
OSCN-G
OSCN-F3
OSCN-F2
OSCN-F1
OSCN-E
OSCN-D
OSCN-C
OSCN-B
OSCN-A
Wonoka
P
N
M
L
K
J
I
H
G
F3
F2
F1
E
D
C
B
A
Vertical scale in meters

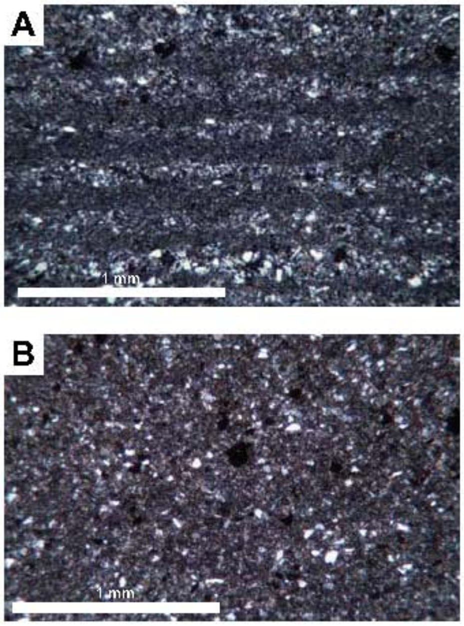
A
1 mm
B
1 mm

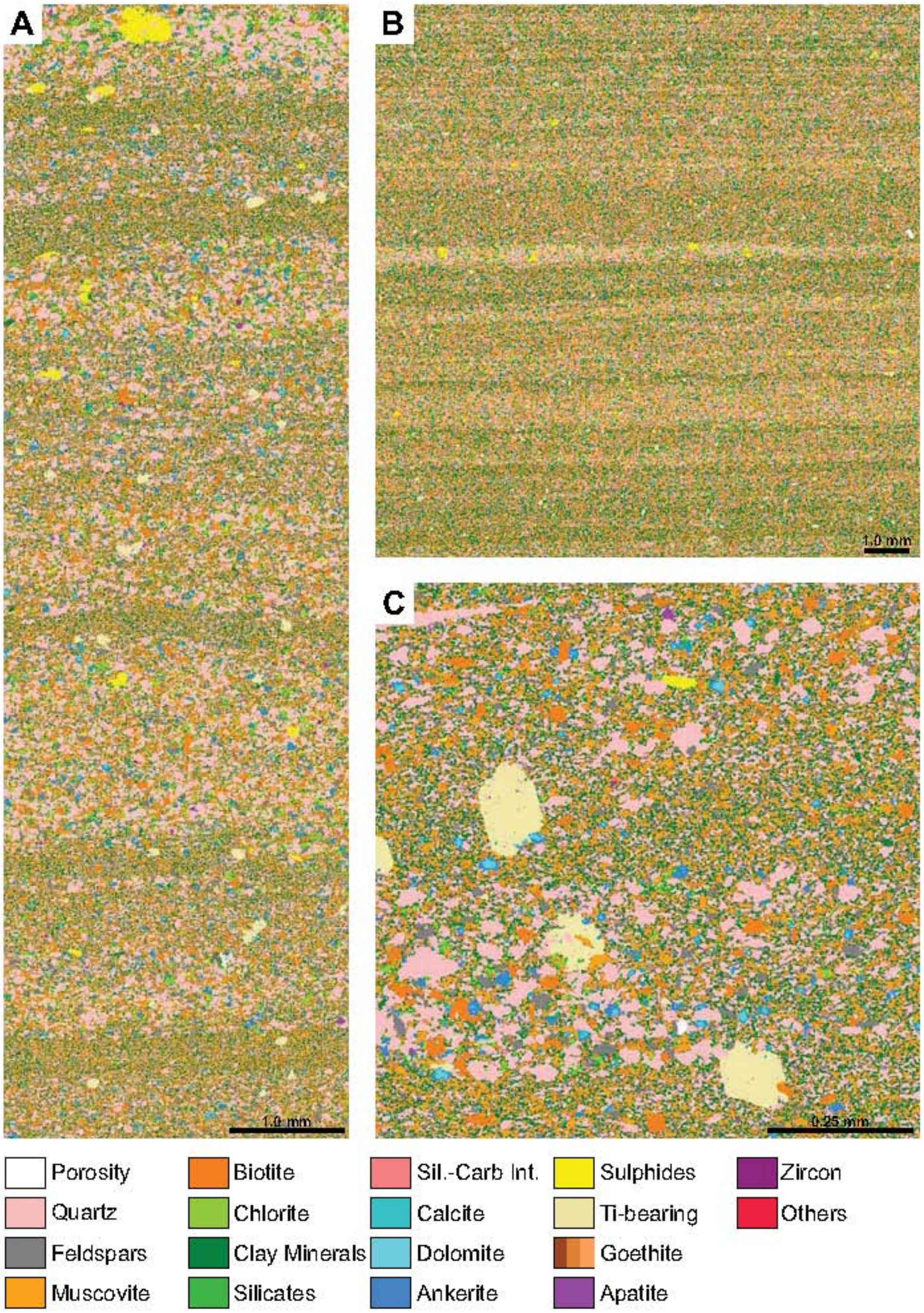
A
B
1.0 mm
C
1.0 mm
0.25 mm
Porosity
Quartz
Feldspars
Muscovite
Biotite
Chlorite
Clay Minerals
Silicates
Sil.-Carb Int.
Calcite
Dolomite
Ankerite
Sulphides
Ti-bearing
Goethite
Apatite
Zircon
Others

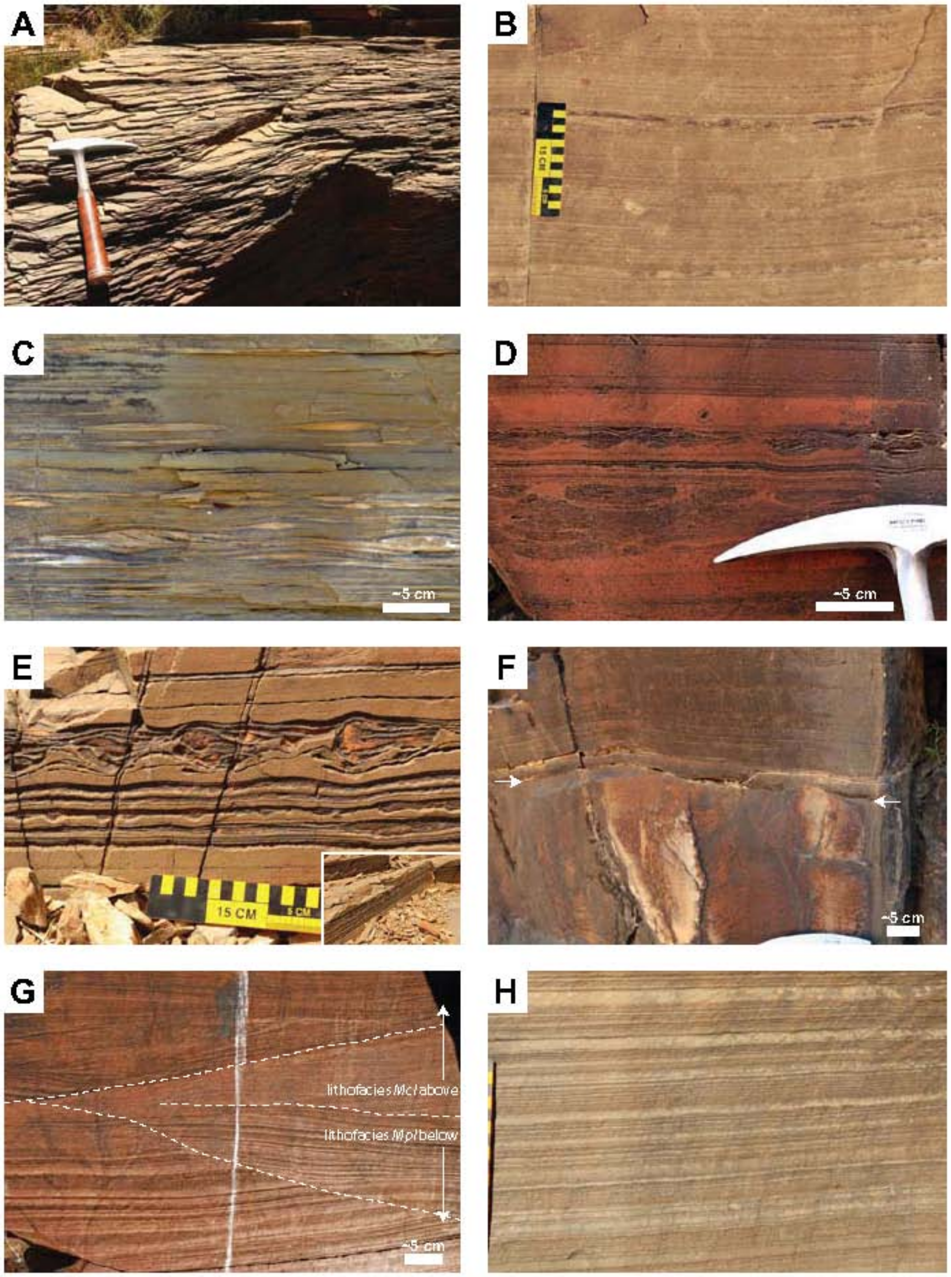
A
B
15 CM
C
~5 cm
D
~5 cm
E
15 CM
5 CM
F
~5 cm
G
lithofacies *Mcl* above
lithofacies *Mpl* below
~5 cm
H

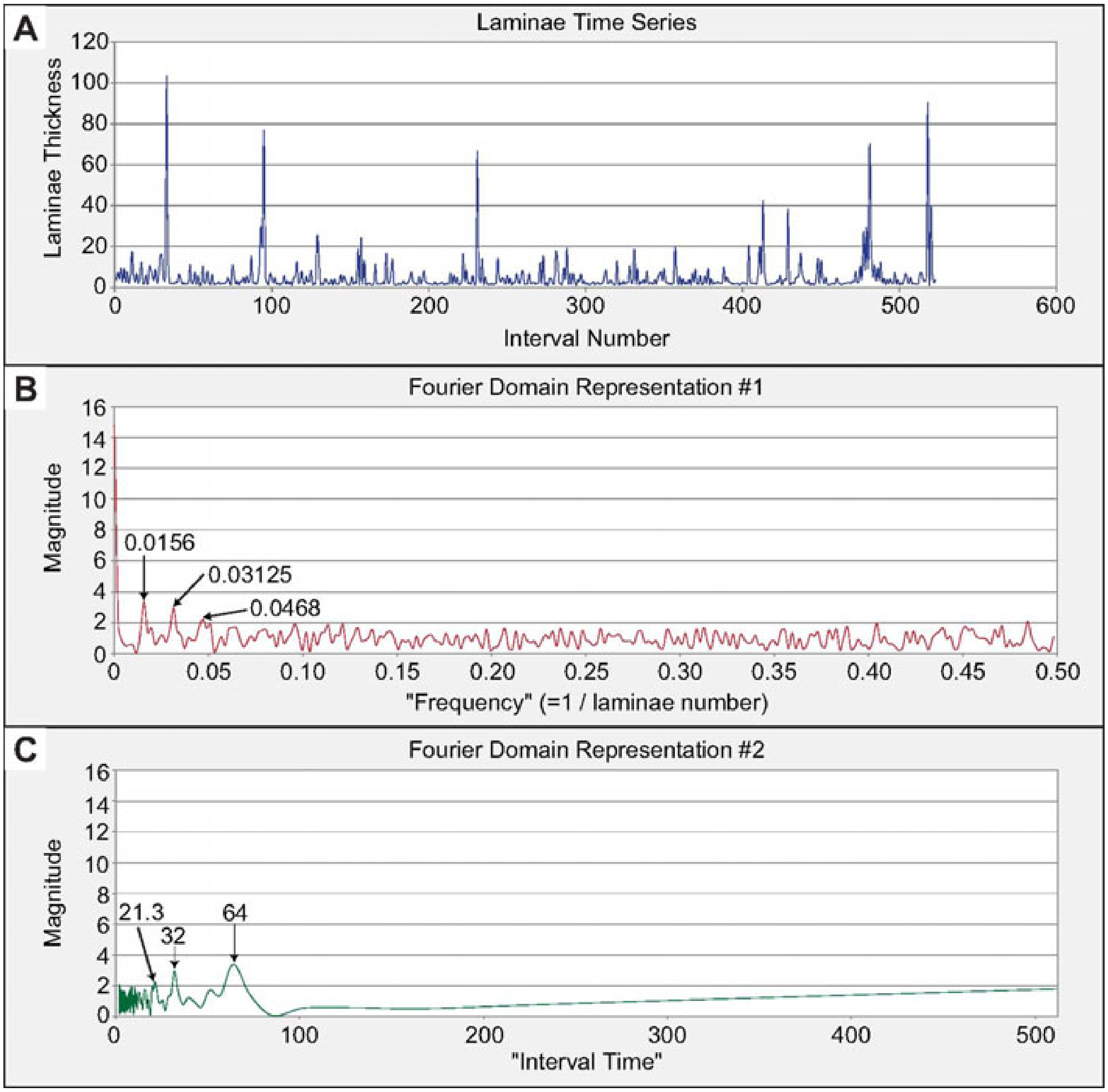
A
Laminae Time Series
Laminae Thickness
120
100
80
60
40
20
0
0
100
200
300
400
500
600
Interval Number
B
Fourier Domain Representation #1
Magnitude
16
14
12
10
8
6
4
2
0
0.0156
0.03125
0.0468
0
0.05
0.10
0.15
0.20
0.25
0.30
0.35
0.40
0.45
0.50
"Frequency" (=1 / laminae number)
C
Fourier Domain Representation #2
Magnitude
16
14
12
10
8
6
4
2
0
21.3
32
64
0
100
200
300
400
500
"Interval Time"

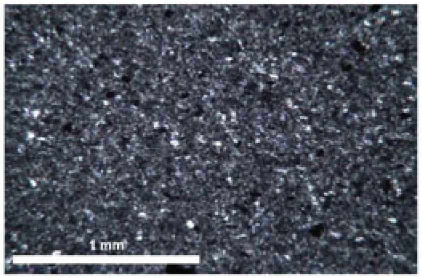
1 mm

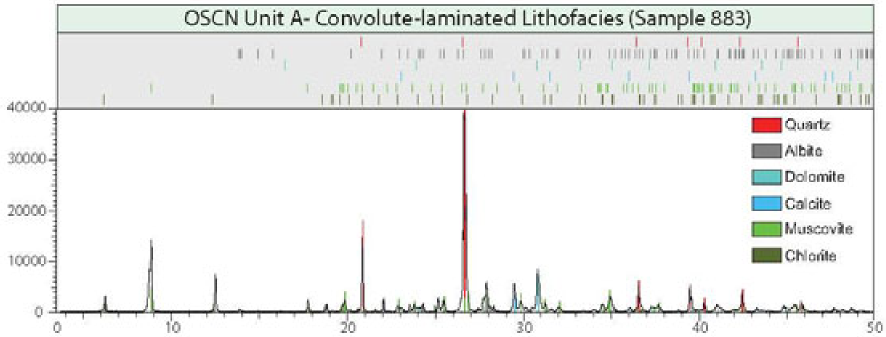
OSCN Unit A- Convolute-laminated Lithofacies (Sample 883)
40000
30000
20000
10000
0
0
10
20
30
40
50
Quartz
Albite
Dolomite
Calcite
Muscovite
Chlorite

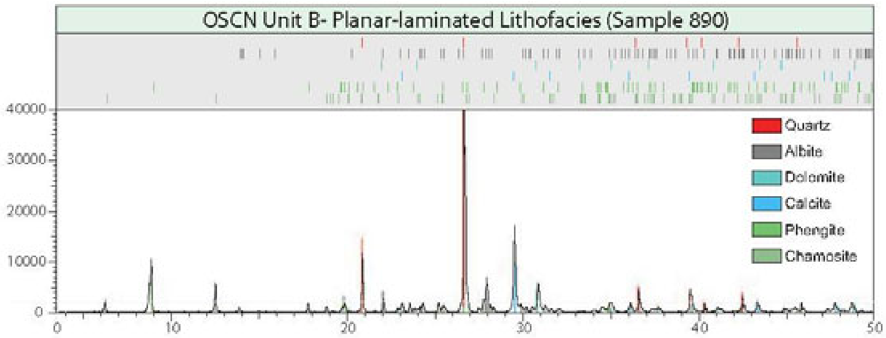
OSCN Unit B- Planar-laminated Lithofacies (Sample 890)
40000
30000
20000
10000
0
0
10
20
30
40
50
Quartz
Albite
Dolomite
Calcite
Phengite
Chamosite

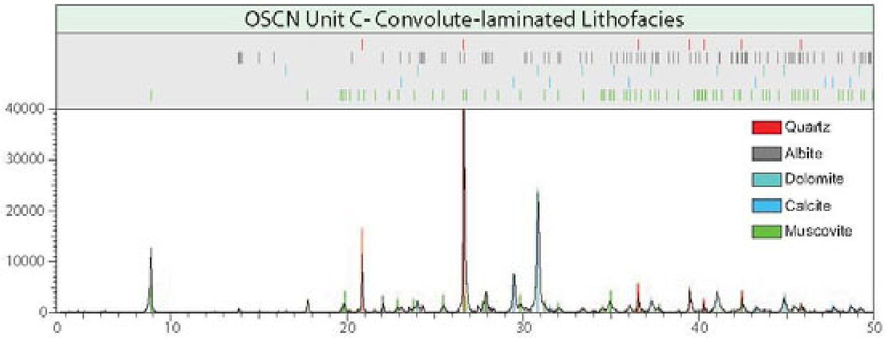
OSCN Unit C- Convolute-laminated Lithofacies
40000
30000
20000
10000
0
0
10
20
30
40
50
Quartz
Albite
Dolomite
Calcite
Muscovite

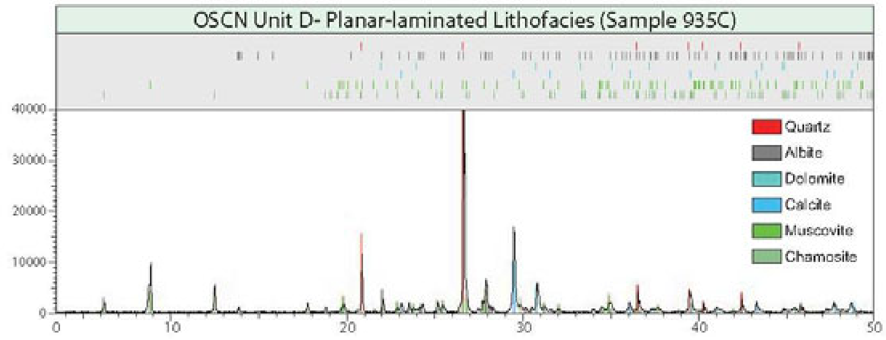
OSCN Unit D- Planar-laminated Lithofacies (Sample 935C)
40000
30000
20000
10000
0
0
10
20
30
40
50
Quartz
Albite
Dolomite
Calcite
Muscovite
Chamosite

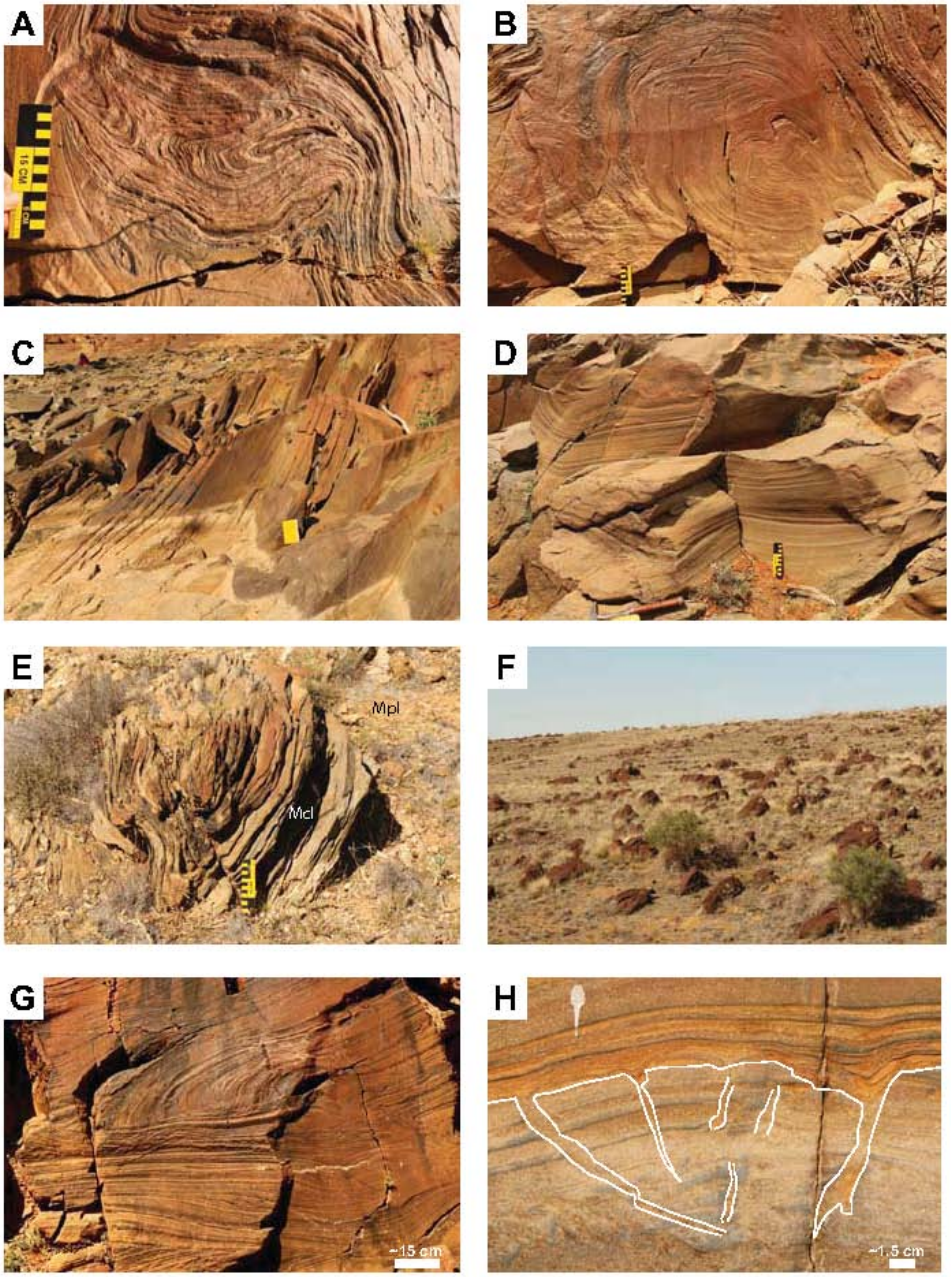
A
15 CM
B
C
D
E
Mpl
Mcl
F
G
~15 cm
H
~1.5 cm

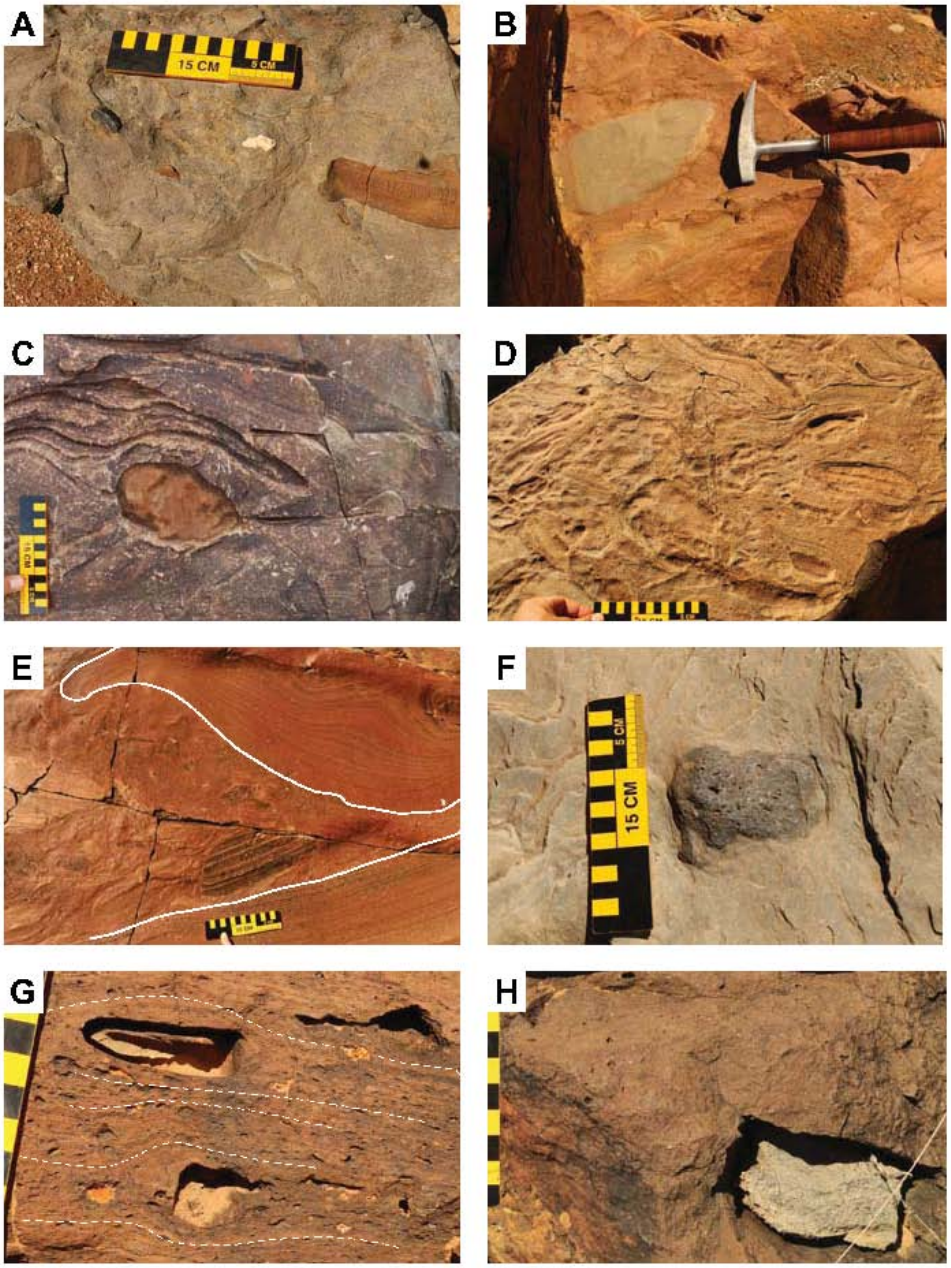
A
15 CM
5 CM
B
C
D
E
F
5 CM
15 CM
G
H

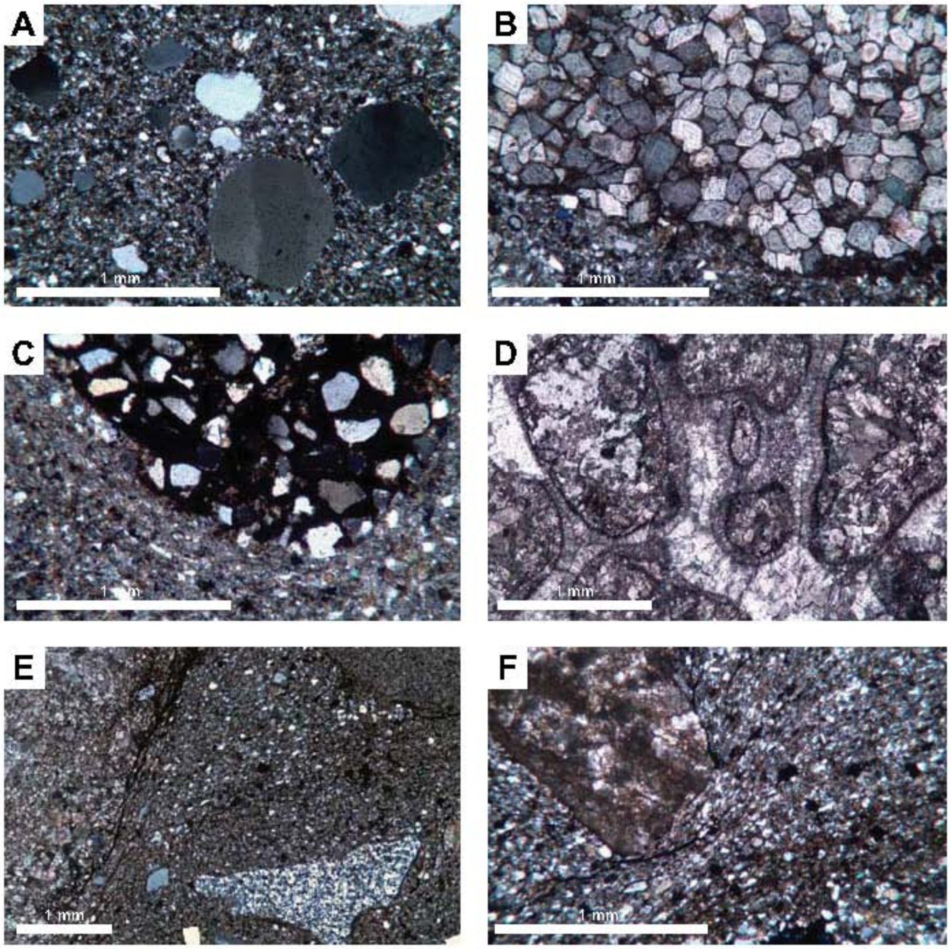
A
1 mm
B
1 mm
C
1 mm
D
1 mm
E
1 mm
F
1 mm

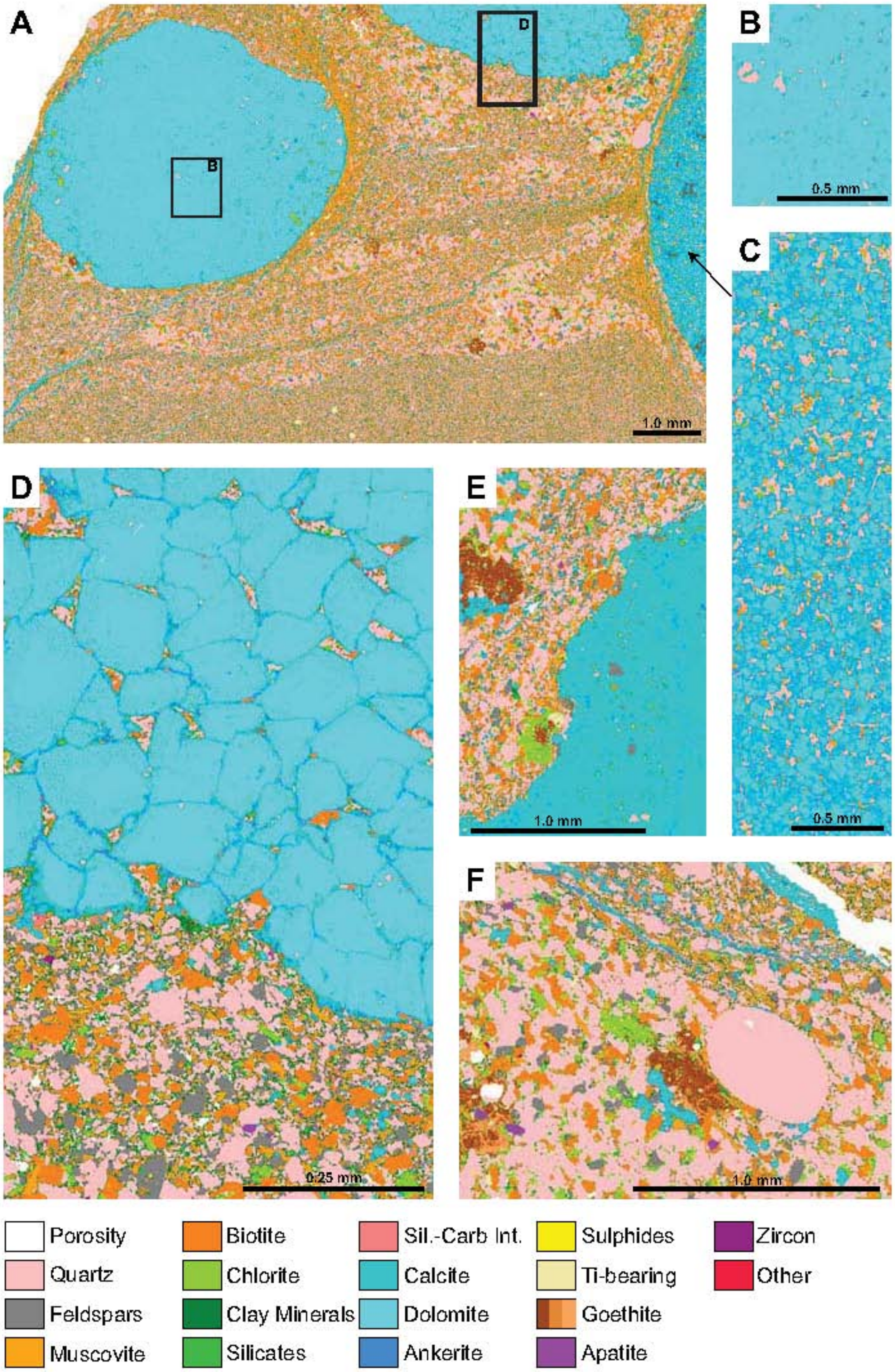
A
D
B
1.0 mm
B
0.5 mm
C
D
0.25 mm
E
1.0 mm
0.5 mm
F
1.0 mm
Porosity
Quartz
Feldspars
Muscovite
Biotite
Chlorite
Clay Minerals
Silicates
Sil.-Carb Int.
Calcite
Dolomite
Ankerite
Sulphides
Ti-bearing
Goethite
Apatite
Zircon
Other

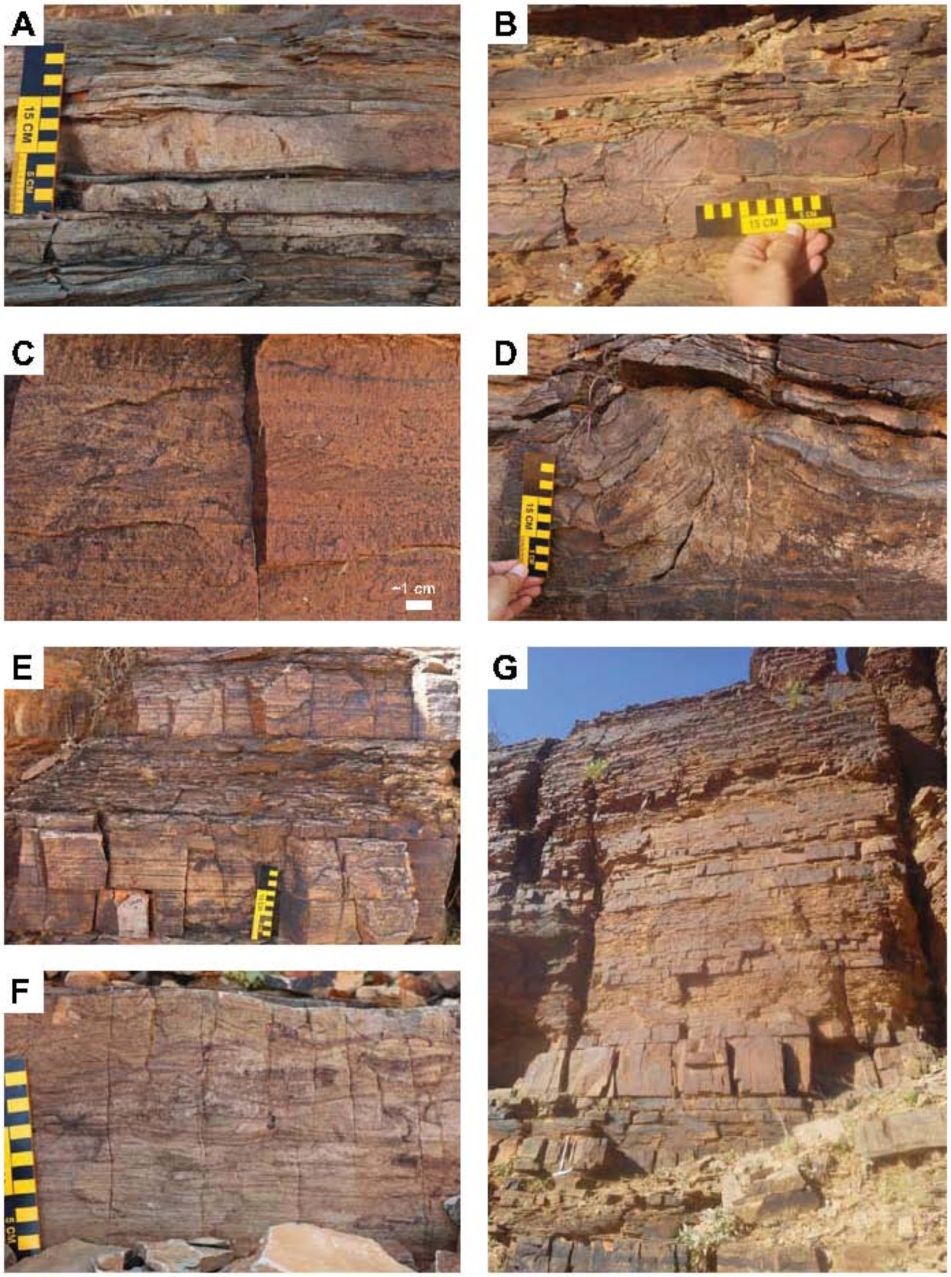
A
15 CM
5 CM
B
15 CM
5 CM
C
~1 cm
D
15 CM
5 CM
E
F
5 CM
G

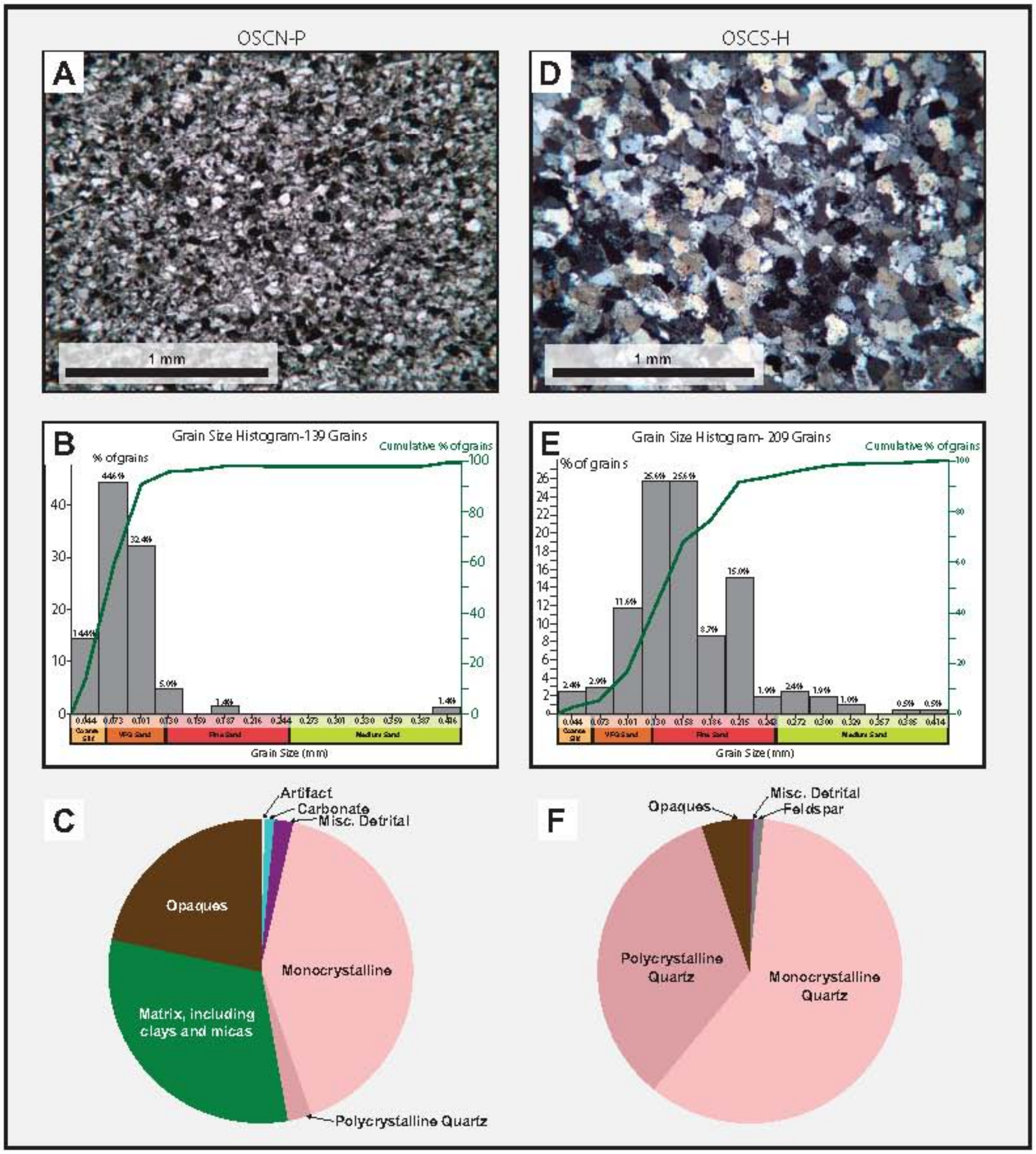
OSCN-P
OSCS-H
A
1 mm
D
1 mm
B
Grain Size Histogram-139 Grains
% of grains
Cumulative % of grains
0
10
20
30
40
14.4%
44.6%
32.4%
5.0%
1.4%
1.4%
0
20
40
60
80
100
0.044
0.073
0.101
0.130
0.159
0.187
0.216
0.244
0.273
0.301
0.330
0.359
0.387
0.416
Coarse Silt
VFG Sand
Fine Sand
Medium Sand
Grain Size (mm)
E
Grain Size Histogram- 209 Grains
% of grains
Cumulative % of grains
0
2
4
6
8
10
12
14
16
18
20
22
24
26
2.4%
2.9%
11.6%
25.6%
25.6%
8.7%
15.0%
1.9%
2.4%
1.9%
1.0%
0.5%
0.5%
0
20
40
60
80
100
0.044
0.073
0.101
0.130
0.158
0.186
0.215
0.243
0.272
0.300
0.329
0.357
0.385
0.414
Coarse Silt
VFG Sand
Fine Sand
Medium Sand
Grain Size (mm)
C
Artifact
Carbonate
Misc. Detrital
Opaques
Monocrystalline
Matrix, including clays and micas
Polycrystalline Quartz
F
Misc. Detrital
Opaques
Feldspar
Polycrystalline Quartz
Monocrystalline Quartz